Identifying and targeting abnormal mitochondrial localization associated with psychosis

FULLY REVISED MANUSCRIPT – NO TRACK CHANGES

Marzieh Haghighi[1]*, Donna McPhie[2]*, Mohammad Rohban[1], Erin Weisbart[1], David J. Logan[1], Kyle W. Karhohs[1], Suzann M. Babb[2], Jessica D. Ewald[1], Johan Fredin Haslum[1], Beth A. Cimini[1], Shantanu Singh[1], Bruce M. Cohen[2]^, Anne E. Carpenter[1]^

1. Imaging Platform, Broad Institute of MIT and Harvard, Cambridge MA USA 02142
2. McLean Hospital, Harvard Medical School

*equal contribution
^ equal contribution, corresponding authors

Abstract

Therapeutics working by novel mechanisms are needed for patients with psychiatric conditions. Cell-based assays to identify candidates that reverse observed abnormalities could accelerate the process. Here, we imaged peripheral cells (skin fibroblasts) of 168 patients, stained for DNA, actin, and mitochondria. We found mitochondria tend to be farther from the cell border for patients who experience psychosis (including subsets of individuals with bipolar disorder, schizophrenia, and schizoaffective disorder). We observed a reverse trend, albeit not statistically significant, for patients diagnosed with major depression. Because the mitochondrial dispersion phenotype could be identified by a single metric, we were able to readily query existing databases of cells stained for their mitochondria and treated with various chemical or genetic perturbations. We identified compounds and genes both negatively and positively affecting the psychosis-associated phenotype, including some known to impact psychiatric conditions. Developing therapeutics with novel mechanisms is a complex multi-step challenge. This cell-based assay holds promise for virtual and physical screening to identify candidates for treating psychiatric conditions.

Introduction

Many patients presenting with psychosis respond only partially or poorly to current treatments. They are in critical need of medicines with novel mechanisms of action, both to improve efficacy and reduce disabling side effects relative to existing medicines (Cohen & Öngür 2018; Stępnicki et al. 2018; McIntyre et al. 2020; Pereira et al. 2018; Kuperberg et al. 2021). These conditions include schizophrenia, schizoaffective disorder and bipolar disorder, which collectively have an enormous economic, social, and emotional impact (Bessonova et al. 2020; Kadakia et al. 2022; Lin et al. 2022).

Unlike many diseases, target-based drug discovery is not ideal for these conditions. Hundreds and even thousands of genes underlie the risk for psychotic disorders, and no single gene determines more than a modest proportion of risk (Trubetskoy et al. 2022). There is limited knowledge about the identity and function of all the proteins and other cellular components involved in the cellular processes that ultimately underlie and lead to psychosis. Current standard medications were discovered serendipitously. Predicting new

protein or cellular targets whose chemical modulation will produce the desired antipsychotic effect in humans, based on existing understanding, is error-prone, making the unbiased approach of phenotypic assays appealing. However, ideal phenotypic assays involve a faithful, high-throughput model of the disease pathogenicity in a dish. This is inherently challenging for conditions involving the brain. Although complex brain organoids can be engineered (Qian et al. 2019; Tan et al. 2021), they are not well-suited to high throughput screening. More importantly, it is unclear what phenotypic effect ought to be sought in cells or organoids in order to identify compounds that relieve neuropsychiatric symptoms. Often, promising therapeutic hypotheses fail in the clinic given complexities at the organism level and a faulty link between a proposed target or phenotype and the human condition.

Rather than starting from a hypothesized phenotype based on existing scientific knowledge for a condition, recent evidence demonstrates that phenotypes can be identified in an unbiased way directly from patient samples, as we discuss next. Association of a cell phenotype with a condition does not prove causation; nevertheless, it enables drug screening, such that compounds reversing cell-based phenotypes are worth testing to see if they effectively reverse disease symptoms.

Patient fibroblasts, derived from a skin biopsy, are an appealing source material for identifying phenotypes because they are a cell type that is relatively accessible, acquirable from living patients, and sufficiently propagated for high-throughput screens. Although some fibroblasts share an origin with neuroectoderm, they would not be expected to have all of the necessary cellular pathways and structures to accurately reflect phenotypes for all human conditions. Still, phenotypes for several neurological conditions have been detected in patient fibroblasts (Olesen et al. 2022). Studies that revealed mitochondrial morphology phenotypes as compared to controls include fibroblasts from 41 patients with mid-stage idiopathic Parkinson's disease (Antony et al. 2020), in several genetic and chemical neuronal models of Parkinson's disease (Thomas et al. 2023), and in 46 patients with Parkinson's – 32 sporadic, 14 carrying particular mutations (Schiff et al. 2022). A change in several mitochondrial functions was found in 100 sporadic Parkinson's patients and 50 age-matched controls (Carling et al. 2020); mitochondrial count and mitochondrial membrane potential phenotypes were also observed in 35 patients with Parkinson's disease and 25 healthy controls (Payne et al. 2024). An increased mitochondrial and lysosome co-localization and an increased rate of mitochondrial collapse were found in sporadic Parkinson's fibroblasts, a phenotype reversible by the LRRK2 inhibitor LRRK2-in-1 (Smith et al. 2016). In spinal muscular atrophy, machine learning could distinguish fibroblast images of 12 patients from 12 healthy controls, though the study could not rule out technical confounders (Yang et al. 2019). SORL1 is a gene associated with Alzheimer's disease; morphology phenotypes distinguished SORL1 knockout neural progenitor cells from isogenic wild-type controls (McDiarmid et al. 2023). 15 people with two genotypes of hereditary spastic paraplegia were distinguished from matched controls using stains for DNA, mitochondria, and acetylated α-tubulin, plus label-free phase contrast cell images in fibroblasts (Wali et al. 2021). Other studies also uncovered phenotypes for neurological conditions in smaller cohorts (Blanchet et al. 2015; Hung et al. 2018; Wali et al. 2023; Teves et al. 2017; Smith et al. 2016; Mortiboys et al. 2008; Mortiboys et al. 2010).

Therefore, although some conditions might only have phenotypes detectable at the organ or organismal level, others do seem to manifest at the peripheral cell level. Similarly, although some disease-related phenotypes might only be visible in a "relevant" cell type, others may be detectable in a broader spectrum of cell types, including fibroblasts. This may be due to the repurposing of many cellular components across diverse functions in different cell type contexts, or because cellular mechanisms may exist and be impacted in a diversity of cell types even though the symptoms experienced by a patient are only observed in a particular organ system, perhaps due to compensatory mechanisms elsewhere. For psychotic disorders, it is notable that patients are at elevated risk for other non-psychiatric disorders and there are substantial overlaps between gene sets associated with the two (Bulik-Sullivan et al. 2015; Andreassen et al. 2013). Therefore, it would not be surprising if peripheral cells showed abnormalities relevant to those in brain cells. Because obtaining live cells from the human brain is rarely possible and because generating relevant neural cell types by either differentiation of hiPSC lines or by direct conversion of somatic cells is challenging at scale (Panchision 2016), identifying phenotypes in cell types that are readily obtained and high-throughput-compatible could accelerate discovery.

In 2010, we reported finding a morphological phenotype in fibroblasts and lymphocytes from 10 bipolar patients as compared to 10 control patients (Cataldo et al. 2010). Specifically, the distribution of mitochondria was unusual in bipolar patients, whose cells displayed mitochondrial networks that were much more dense and concentrated near the nucleus, versus controls whose mitochondria dispersed more evenly throughout the cell.

The finding of morphological abnormalities in mitochondria of patients with conditions producing psychosis is now affirmed by a wide variety of genetic, brain imaging, and peripheral cell studies (Scaini et al. 2021; Flippo & Strack 2017; Papageorgiou & Filiou 2024). Postmortem brains of bipolar patients have more, but smaller, mitochondria (Cataldo et al. 2010), as do their fibroblasts *ex vivo* (Marques et al. 2021) and iPSC-derived neurons, *in vitro* (Mertens et al. 2015). Mitochondrial fragmentation is also seen in Epstein-Barr virus (EBV)-transformed lymphocytes from schizophrenic patients (Rosenfeld et al. 2011). Similar glutamate-induced fragmentation can be mitigated in mouse hippocampal HT22 cells when the psychiatric disorder-associated gene CACNA1C (Moon et al. 2018; Sklar et al. 2008) is knocked down by RNA interference (Michels et al. 2018). Postmortem brains of patients with schizophrenia show a lower density of mitochondria in axon terminals, compared to healthy brains (Roberts 2021). Evidence for functional abnormalities in mitochondria is even more solidly associated with these conditions, ranging from genetics (Cuperfain et al. 2018), alterations in mitochondrial fusion/fission proteins (Scaini et al. 2017), bioenergetics (Zanfardino et al. 2021), mitochondrial membrane potential (Marques et al. 2021; Munakata et al. 2004; Brennand et al. 2015; Robicsek et al. 2013), and more (Scaini et al. 2021; Wu et al. 2019; Scaini et al. 2016; Pereira et al. 2018; Kuperberg et al. 2021; Giménez-Palomo et al. 2021). Likewise there is evidence for morphological and functional impairment of mitochondria in major depressive disorder (Culmsee et al. 2018; H. Chen et al. 2024). Collectively, these findings are consistent with the more general conclusion that mitochondrial morphology and function are tightly related and abnormal in many psychiatric conditions (Chan 2020; Bulthuis et al. 2019; Jenkins et al. 2024; Ni et al. 2024).

Here, we sought to increase confidence in a mitochondrial localization phenotype in psychiatric conditions by testing a new, larger cohort: 168 people as compared to our original set of 20. Indeed, the lack of attempts to replicate findings in larger cohorts has been described as limiting progress in the field (Harrison et al. 2020). We also sought to expand the study to related psychiatric conditions beyond bipolar disorder - for the past fifteen years, we have been collecting samples from patients experiencing psychosis across a spectrum of conditions including schizophrenia, schizoaffective disorder and bipolar disorder, along with healthy control patients and patients with major depressive disorder. Finally, because computational analysis of images has advanced dramatically in the past decade and public datasets are now available, we were also able to develop and pilot a virtual screening approach based on mitochondrial localization that might identify chemical and genetic perturbations relevant to the psychiatric conditions in other datasets.

Results

Mitochondrial localization is disrupted in fibroblasts from patients experiencing psychosis

We sought to identify a morphological phenotype in a cohort of patients experiencing psychosis. Such a phenotype could subsequently be used to screen public image datasets to identify potential therapeutics; that is, agents that impact the illness-related phenotype (Figure 1). We collected skin punch biopsies from patients and derived human fibroblasts from them, including from 50 people with a primary diagnosis of bipolar disorder (BP), 38 with schizophrenia (SZ), 11 with schizoaffective disorder (SZA), 1 with psychotic disorder not otherwise specified, 20 with major depressive disorder (MDD), and 47 healthy controls; together with patient demographic metadata including their primary diagnosis. The median and range of ages was consistent across patient categories, as was the typical male-skewed ratio seen for these conditions, except for MDD (Supplementary Figure 1). We chose fibroblasts for their benefits described in the introduction; furthermore, schizophrenia and bipolar disorder have known associations with skin abnormalities (McPhie et al. 2021), serving as additional rationale that this cell type may exhibit disease-associated phenotypes. We grew the cell lines as consistently as possible prior to plating, fixing, staining them for DNA, actin, and mitochondria (using MitoTracker Orange-M7510), and imaging them (Figure 2). By eye, we observed that samples from patients in the control and MDD categories show a dispersed mitochondrial network composed of thin filaments extending to the cell periphery, whereas patients in the categories experiencing psychosis tend to show an agglomerated, network of thicker tubules concentrated closer to the nucleus. The pattern is subtle and heterogeneous across a cell population. We next sought metrics to quantify these observations objectively, consistently, and efficiently, hoping we could use the resulting phenotype for screening existing public datasets.

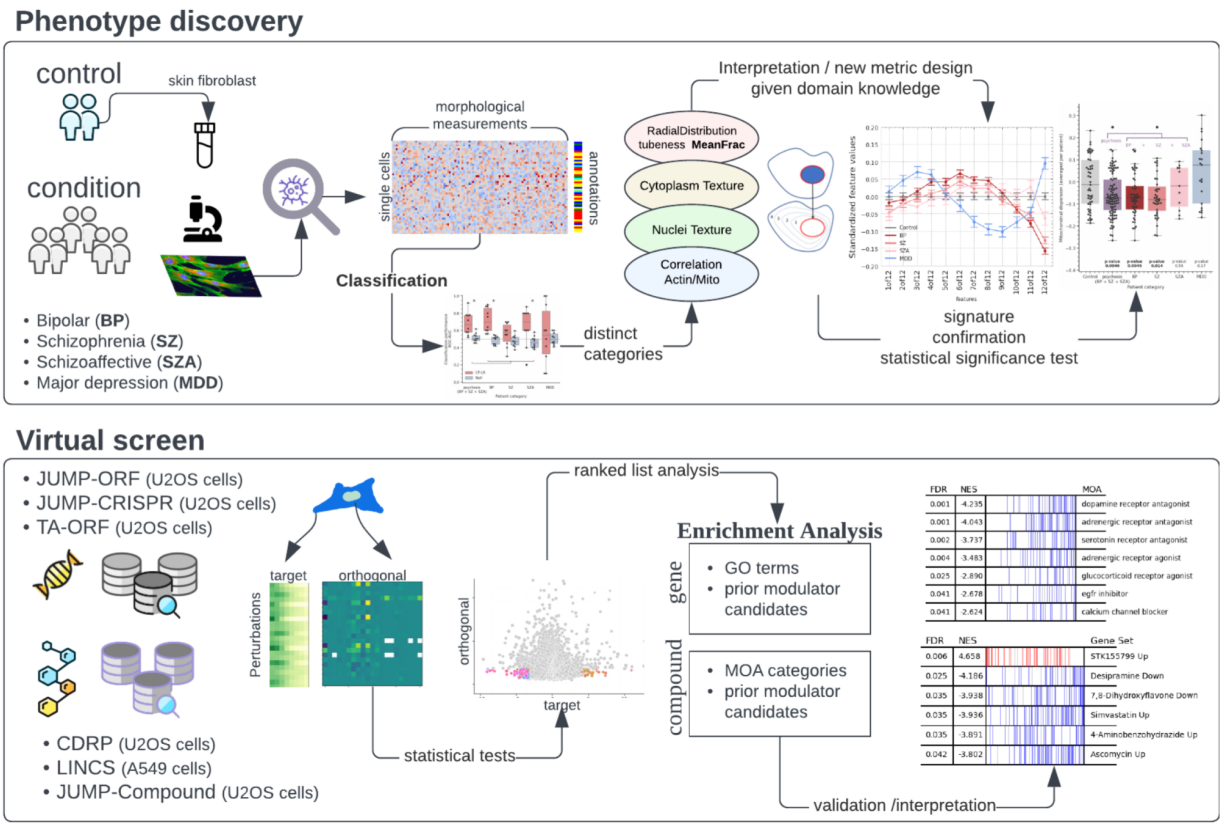

Figure 1: Overview of our strategy for phenotype discovery and virtual screening.

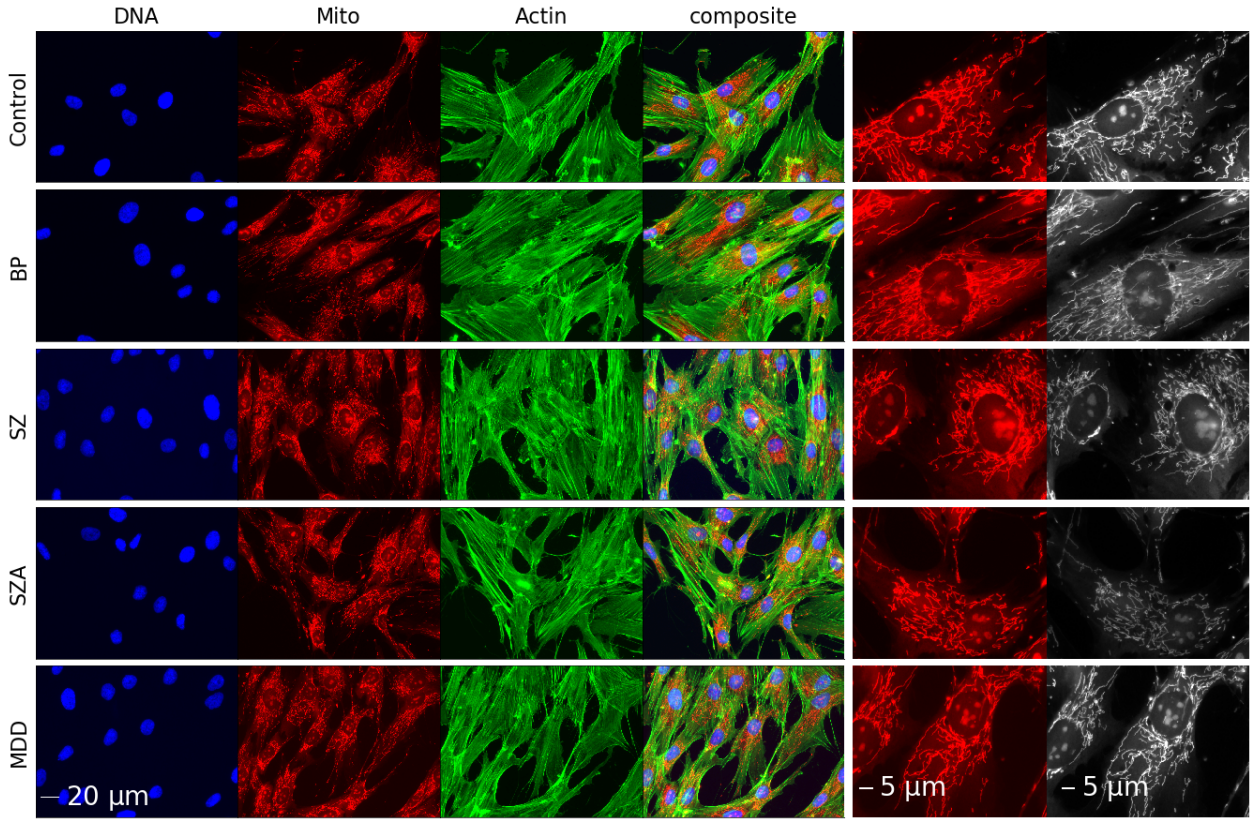

Figure 2: Morphological phenotypes associated with psychiatric conditions are visible but subtle. *Fibroblasts that are stained for DNA, actin, and mitochondria, and labeled according to the patient category. Representative images were selected by identifying the subject closest to the median MITO-SLOPE for each group, then choosing the image from that subject with a MITO-SLOPE closest to the group median; the larger field of view shows the phenotype more clearly. Color images are clipped to their 0.5 and 99.5 percentile of their range and scaled to [0, 255] range just for visual clarity, given that the overall intensity of the staining is not the phenotype to be observed here. The grayscale images of mitochondria in the last column are scaled individually to the min/max, again just for display. Scale bar = 20 µm for the first four images in each row, which are full fields of view. Cropped images of MitoTracker in the last two columns have a scale bar of 5 µm.*

To preserve interpretability, we used classical image processing techniques to extract well-understood features of morphology, which include measures of size, shape, intensity and texture of the cell components observed using the various stains (Stirling et al. 2021). Machine learning classifiers were able to distinguish BP, SZ, and SZA patient groups from healthy controls using linear regression; the combination of these three groups who all experience psychosis was also distinguishable (Figure 3). The strongest phenotypes were seen in patients with the affective conditions, BP and SZA. This may be consistent with the observation that such patients, especially those in a manic episode, have the most extreme episodes of psychosis with so-called 'positive' symptoms, observed as hallucinations, delusions and agitated behavior (Carlson & Goodwin 1973). A convolutional neural network

based on raw images' pixels yielded roughly similar results (Supplementary Figure 2). By contrast, the MDD patient group was the least distinguishable from healthy controls. Unlike diseases whose phenotypes readily and completely separate patients from controls, we were not surprised that phenotypes for these mental conditions were subtle: most patient groups were not completely distinguishable from healthy controls in all folds of our 10-fold cross validation run. This is expected given genetic, diagnostic, and environmental variability among patients, as well as the fact that dramatic changes in cell phenotypes would likely be associated with death in utero or early and substantial cognitive impairments such as those seen in neurodevelopmental disorders. We believe that risk of illness is likely determined by more than mitochondrial distribution alone, yet this phenotype could be useful for drug screening.

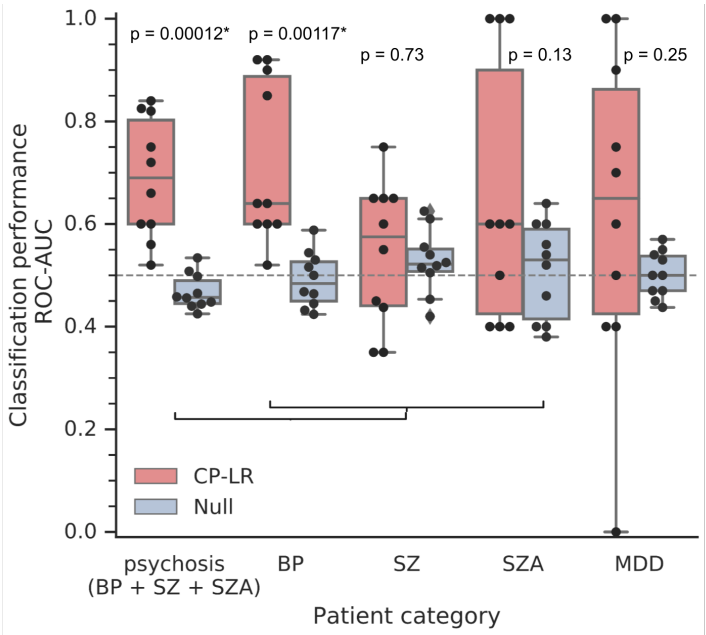

Figure 3: Machine learning classification based on multiple mitochondrial features distinguishes patient group experiencing psychosis from healthy controls*. Logistic Regression (LR) classifiers were trained on patient-level profiles constructed from mitochondrial features extracted using CellProfiler (CP) software (CP-LR). Patient categories include those with a primary diagnosis of bipolar disorder (BP), schizophrenia (SZ), schizoaffective disorder (SZA), and major depressive disorder (MDD). Psychosis encompasses patients in the BP, SZ, and SZA groups. Classifier performance is evaluated using 10-fold cross-validation, with the distribution of the area under the receiver operating characteristic curve (AUC-ROC) for each binary classification shown as individual data points on the box plots. The box plots represent the interquartile range (25th–75th percentile), with the median marked by a horizontal line. The null distribution (blue) was generated by training classifiers on shuffled patient class labels. Statistically significant differences between classifications (e.g., psychosis vs. healthy) are denoted by*

asterisks. The cellular features captured here are most prominent in participants with affective psychoses, BP and SZA.

We routinely use machine learning, including deep learning, to detect morphological phenotypes in images, and others have used machine learning to distinguish disease-associated samples (see Introduction). These strategies leverage hundreds to thousands of features. However, it is preferable for screening purposes for the phenotype to be a single feature. A single feature (or a combination of a few) is more readily translatable across cell types and experimental batches, including existing publicly available datasets. Keeping the number of features low is also valuable to conserve statistical power and avoid overfitting that can occur when measuring thousands of morphological features for only dozens of samples (Lones 2021).

We therefore sought a simpler morphological metric for the phenotype associated with these psychosis-related conditions of interest. Many metrics exist to measure the properties of mitochondrial networks (Leonard et al. 2015; Hemel et al. 2021; Harwig et al. 2018; Chu et al. 2022); some rely on segmentation, where the boundaries of individual mitochondria are identified and measured for properties such as area, aspect ratio, and circularity, as well as their position relative to the nucleus, cell edge, or each other. However, this was ineffective in our patient fibroblast images, where most of the mitochondrial mass is organized in more filamentous and interconnected fashion rather than as distinct objects. More problematically, we planned to use the metric to virtually screen existing genetic and chemical image sets that are much lower-resolution, making segmentation of mitochondria impossible.

We therefore designed a metric called MITO-SLOPE to capture the phenotype based on the data, our prior study (Cataldo et al. 2010), and robustness across datasets. MITO-SLOPE is fundamentally a localization metric that quantifies the gradient of change in mitochondrial network density towards the cell edge (Figure 4, with details in Methods), where the cell edge is defined by available cytoplasmic stains, which vary across the image sets in this study. We used MitoTracker Orange (M-7510) at a moderate concentration; nevertheless we observed nuclear/nucleolar staining which is a documented phenomenon (Qi et al. n.d.); however, nuclear staining is ignored in the MITO-SLOPE metric.

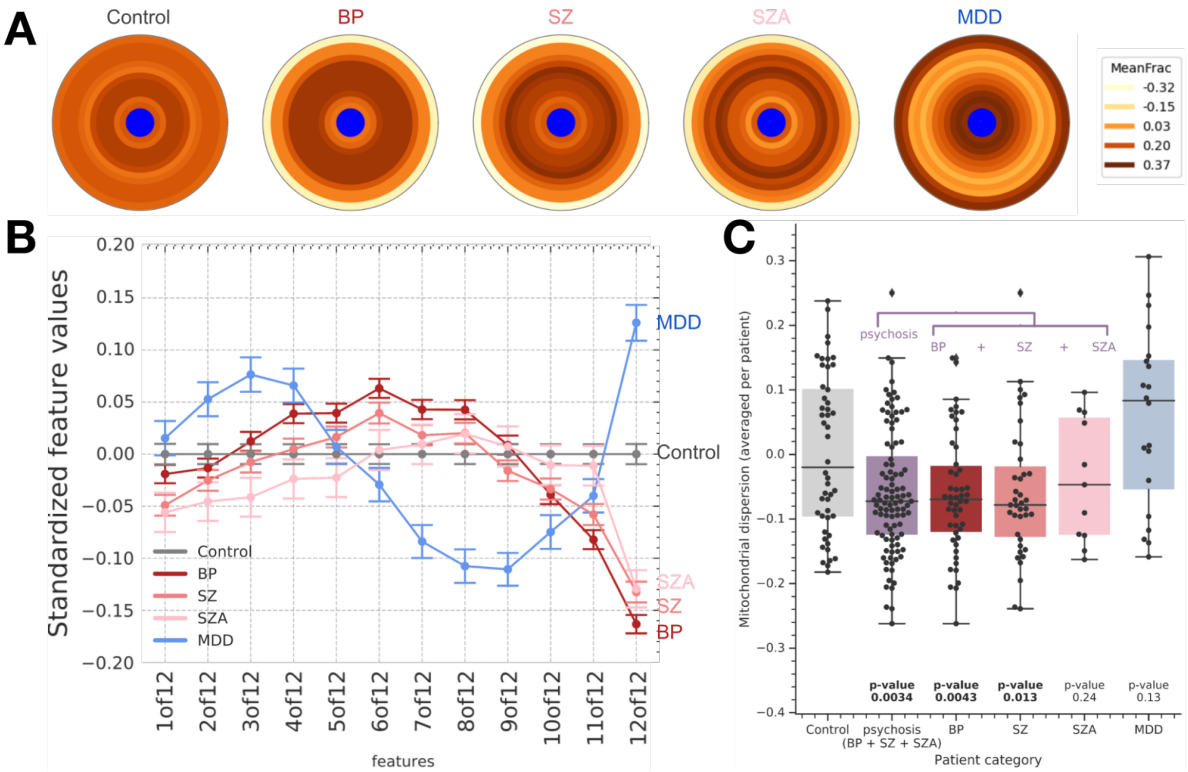

Figure 4: Localization of mitochondria differs in various patient groups experiencing psychiatric conditions*. (A) Localization features computed for MitoTracker staining (after a tubeness transformation, Methods): the fraction of staining is measured in each of 12 concentric rings from the nucleus (blue schematic) to the cell border. The metric is named Cells_RadialDistribution_MeanFrac_mito_tubenessNNof12 where NN is the bin number, and "MeanFrac" is normalized by the fraction of pixels at a given radius and also z-scored across the experiment. MITO-SLOPE is defined as the slope of change for this feature towards the cell periphery (see Methods for definition), relative to control patients (for all patient groups, mitochondrial staining lessens towards the cell periphery, so we analyze relative changes). Note that for the Control group, values are not precisely zero because each ring represents a distribution of normalized values that center around 0 coming from a population of individually normalized single cells. Because the individually-normalized profiles are aggregated to a single per-patient-category value, we expect the "control" profile to be close to 0 but not actually 0 due to the biological variability in the single cells. Because the bin size adapts to the size of each cell, MITO-SLOPE is inherently normalized to cell size and because MITO-SLOPE is based on the fraction of mitochondrial staining in each bin, it is inherently normalized to the total intensity of staining for each cell. (B) Mean standardized values (± standard error) across the 12 bins, ordered from the edge of the nucleus (1of12) to the cell periphery (12of12), and standardized to the control group. Patients with bipolar disorder (BP, dark red) and schizophrenia (SZ, red) show a declining pattern at the cell periphery, indicating reduced mitochondrial density near the cell edge. In contrast, major depressive disorder (MDD, blue) shows increased peripheral mitochondrial signal. (C) The value of the MITO-SLOPE feature representing mitochondrial dispersion is shown for each patient (derived from the mean-averaged pattern across the cells within each patient) in each category. "Psychosis"*

includes the patients in the categories BP, SZ, and SZA. Box plots show the median and upper and lower quartiles and whiskers denote the 1.5× interquartile range. P-values are noted for each comparison to the control group.

For all patient groups, mitochondrial staining is higher at the edge of the nucleus and decreases towards the cell edge - however, the *relative* staining intensity compared to controls, as measured by MITO-SLOPE, differs. Specifically, MITO-SLOPE is decreased (relative to healthy controls) for patients who experience psychosis ($p = 0.0034$), particularly the subsets of that group with bipolar disorder ($p = 0.0043$) and schizophrenia ($p = 0.013$) (Figure 4C). This means their mitochondria are not strongly localized at cell edges, relative to controls. MITO-SLOPE for the schizoaffective disorder subset of patients shows a trend in the same direction but with a p value of 0.24; this category had the smallest number of patients (11). Patients with depression show a non-statistically-significant trend ($p = 0.13$ - the second smallest category, with 20 patients) in the opposite direction, with mitochondria showing a relative increase at the edge of the cell. Again, we note that individual patients' values for the phenotype overlap the healthy controls and each other; this is not surprising given that environmental factors contribute to risk and given that these diagnoses are not as dramatically distinctive as, for example, the other neurological disorders mentioned in the introduction, where in some cases only a dozen samples were sufficient to distinguish the condition. We also note that although metrics of cell size are somewhat correlated with MITO-SLOPE, these do not distinguish patient categories (Supplementary Figure 3A-E), nor does the weighted average of mitochondrial intensity in concentric rings, although it is more strongly correlated with MITO-SLOPE (Supplementary Figure 4A). Some skeleton-based metrics do differentiate, but less powerfully than MITO-SLOPE (Supplementary Figure 4B).

These findings are consistent with our prior published results on 10 bipolar patients (Cataldo et al. 2010) but expands to a larger number and includes other conditions that present with psychosis, such as schizophrenia. It is also consistent with our prior work that found a mitochondrial localization phenotype in patient astrocytes for a schizophrenia-predisposing syndrome associated with 22q11.2 deletion (Tegtmeyer et al. 2024).

Mitochondrial membrane potential is lower in fibroblasts from patients experiencing psychosis

The MitoTracker™ Orange CMTMRos dye that we used to measure location has also been used to measure mitochondrial membrane potential (MMP) by measuring its total intensity in the cytoplasm of the cell (Yatchenko & Ben-Shachar 2021). In our patient cohort, we observed a decrease in cytoplasmic MitoTracker staining in cell lines associated with psychoses and an increase in staining in cell lines associated with MDD (Supplementary Figure 4C, though MDD is not statistically significant). This is consistent with prior studies demonstrating decreased MMP in bipolar disorder (Marques et al. 2021; Munakata et al. 2004) and in schizophrenia (Robicsek et al. 2013; Brennand et al. 2015).

Chemical regulators of mitochondrial localization

Large public image datasets are becoming available, enabling an intriguing possibility: chemical regulators of relevant pathways, and potential therapeutics, might be identified by assessing disease-associated phenotypes in existing datasets of compounds. Virtually screening existing datasets saves significant cost and time relative to setting up and conducting physical experiments, and such screening has proven effective in identifying promising chemical regulators (Rohban et al. 2022) and therapeutic candidates (Cuccarese et al. 2020). There are caveats. The approach might not work well if the available data are from a different cell type than the cell type where a disease phenotype was identified. However, our ability to find a psychosis-associated phenotype in skin cells, for patients experiencing a neurological anomaly, provides a hint that this phenotype may be present in many cell types. A virtual screen could also fail if effective chemicals are missed because they would only reverse a phenotype in patients' cells that show the phenotype and not show any impact on cells from people not having a psychotic disorder (as is likely the case for most cultured cell lines used in public databases).

Image-based screens, where compounds are physically tested for reversion of a disease-associated phenotype of interest, are very common. However, only recently has image-based *virtual* (or *inferential*) screening been demonstrated (Rohban et al. 2022; Anon 2021; Celik et al. 2024; Neumann et al. 2024). To our knowledge, a large image-based virtual screen based on a phenotype uncovered in patient fibroblasts has not been attempted. The strategy is analogous to connectivity mapping using transcriptional profiles. For example, a recent study reported using post-mortem transcriptional signatures to virtually query the large Connectivity Map gene expression database to identify 35 drugs that target genes associated with the shared risk pathways across BP and SZ, including some that interact with CACNA1D (Grotzinger et al. 2023).

We therefore queried existing Cell Painting datasets. We began with the LINCS dataset cpg0004-lincs (Way et al. 2022) because it includes mostly approved drugs, allowing us to analyze drug categories known to treat certain symptoms for patients with schizophrenia and bipolar disorder. A colleague manually annotated such drugs into various categories based on their mechanisms (Dr. Rakesh Karmacharya, see Acknowledgements), and we found that none of the known psychoactive categories we annotated were statistically enriched in either direction in our ranked list of phenotype strength (Figure 5). This result is consistent with our previous finding that mitochondrial localization in fibroblasts was not impacted by lithium treatment, nor did patients' lithium use alter mitochondrial morphology in postmortem brain samples (Cataldo et al. 2010). We note that existing drugs typically do not clearly and specifically target a single protein or process, so these annotated categorizations are imperfect. Further, fibroblasts do not likely express high levels of the proteins that are the direct targets of most of these psychiatric drugs, nor are fibroblasts part of circuits equivalent to the neural networks that mediate the clinical effects of these drugs. In addition, the therapeutic effects of drugs used for psychosis and depression develop over weeks of treatment. Nevertheless, this affirms that the assay has the potential to identify candidate therapeutics working by a novel mechanism of action that does not clearly map to existing drug categories.

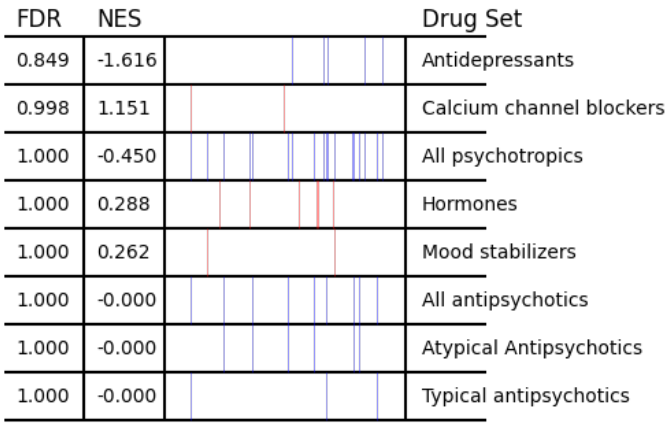

Figure 5: Existing classes of psychoactive drugs do not, overall, show evidence of impacting mitochondrial localization. *For drug mechanism-of-action classes with more than four compounds present in the dataset, we assessed their impact on the mitochondrial localization phenotype, as measured by the mean value of MITO-SLOPE feature across all cells in the sample. The vertical lines in each row represent the positions of individual compounds from that drug class within the ranked list of all compounds ordered by MITO-SLOPE values. None of the mechanism-of-action classes shows a statistically significant rank ordering (in either direction) relative to the other compounds in the assay. NES: normalized enrichment score (red indicates positive NES: more towards the top of the list of compounds rank-ordered by MITO-SLOPE from positive to negative; blue indicates the class is enriched at the negative end of the list - though, again, none of the categories was statistically significantly enriched); FDR: false discovery rate from Benjamini-Hochberg multiple hypothesis correction across all eight drug classes (see Methods). To avoid loss of signal from samples treated with very low concentrations of each drug, we selected (for each compound) the dose that yielded the strongest impact on this phenotype. Results for all classes of compounds and all doses independently are shown in Supplementary Figure 5. All data were cell-count-corrected.*

We then virtually screened the LINCS dataset to find "hits", drugs that impact MITO-SLOPE strongly in either direction. We quickly noticed that many cancer drugs yield strong changes in MITO-SLOPE but also change many other features of cells that would likely lead to adverse outcomes, and would therefore be undesirable for a drug to treat a chronic mental health condition. We therefore designed a strategy to filter hits to only keep those that minimally change morphology of cells within the intersection of two feature subspaces: (1) features that are orthogonal (do not correlate) to mitochondrial localization, and (2) features that are not distinctive across patient groups in the fibroblast dataset (see Methods).

We found seven positive MITO-SLOPE hits (with potential to revert the psychosis phenotype) and three negative hits (with potential to revert a depression phenotype, if

indeed the conditions are at opposite ends of a mitochondrial-localization spectrum) (Figure 6).

A

Common name	Annotated mechanism of action	Dose (uM)	d_slope (mito)	p_slope_std	p_orth_std (other)	mean cell count	Broad Inst. Chemical ID
clioquinol	chelating agent	0.04	0.96	0.00144	0.07	310	BRD-K09255212-001-16-6
clioquinol	chelating agent	0.37	0.68	0.00082	0.06	303	BRD-K09255212-001-16-6
XL-147	PI3K inhibitor	0.12	0.85	0.00000	0.12	313	BRD-K95901403-001-04-5
divalproex-sodium	GABA-potentiating mood stabilizer|HDAC inhibitor	0.04	0.77	0.00001	0.12	265	BRD-K41260949-236-16-8
tivozanib	VEGFR inhibitor	0.04	0.75	0.00618	0.08	323	BRD-K53414658-001-08-2
trapidil	PDGFR tyrosine kinase receptor inhibitor	0.04	0.73	0.00494	0.13	275	BRD-K95763993-001-19-3
ataluren	CFTR channel agonist|dystrophin stimulant	0.04	0.72	0.00011	0.06	335	BRD-K94830329-001-03-0
tolcapone	catechol O methyltransferase inhibitor	0.12	0.70	0.00090	0.05	267	BRD-K10852020-001-04-5
PF-02545920	phosphodiesterase inhibitor	3.33	-0.90	0.00005	0.05	215	BRD-K31519811-001-02-2
cepharanthine	NFkB pathway inhibitor	0.37	-0.52	0.00383	0.67	285	BRD-K96194081-001-10-2
citalopram	selective serotonin reuptake inhibitor (SSRI)	1.11	-0.51	0.00000	0.21	316	BRD-A47598013-004-16-0

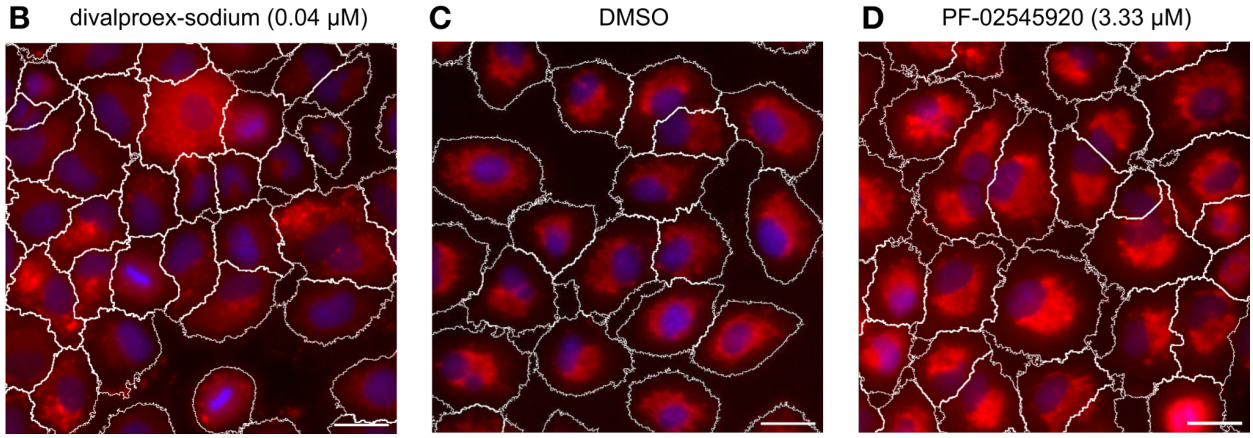

Figure 6: Chemical hits in virtual screen impact mitochondrial localization while minimally impacting cell morphology overall*. (A) The table shows compounds that increase (blue) or decrease (red) mitochondria towards the edge of the cells as measured by d_slope (d_slope is the Cohen's d of the t-test comparing the negative control versus drug-treated cell population, standardized for sample size; the directionality matches the mean of the original values MITO-SLOPE, and the value matches the strength MITO-SLOPE). p_orth_std measures whether non-mitochondrial-related features were significantly different from controls; a filter of 0.05 (after adjusting for multi-hypothesis testing) was applied to ensure the remainder of cell morphology remained fairly normal (see Methods). Of note for drug toxicity, the hits do not dramatically impact cell count, within the time frame of the experiment. Values were calculated for each compound's dose independently. Annotated mechanisms are from the Drug Repurposing Hub. (B) and (C) Representative images of selected hits from the LINCS dataset showing A549 cells treated with (B) 0.04 μM divalproex-sodium showing mitochondria spread throughout the cytoplasm, including the cell edge, (C) DMSO vehicle negative control, and (D) 3.33 μM PF-02545920 showing mitochondria condensed towards the nucleus. The LINCS images also contain endoplasmic reticulum, plasma membrane, f-actin, RNA, and Golgi apparatus stains (not shown) that were used during image analysis for segmenting cell borders (white outlines); blue = DNA, red = MitoTracker. Image intensities displayed in the figure were rescaled relatively for each image (using the minimum/maximum of each image - see*

Methods) for better visualization of the staining pattern but were not rescaled for data analysis. Scale bars = 25 micrometers.

Among the hits, a few drugs are used for psychiatric or neuropsychiatric conditions. Citalopram is a selective serotonin reuptake inhibitor (SSRI) used to treat depression (Sharbaf Shoar et al. 2025); it shows a negative MITO-SLOPE which is the direction expected to normalize the dispersed mitochondrial localization associated with depression. Divalproex-sodium increases gamma-aminobutyric acid (GABA) levels, likely through GABA synthesis, and is an HDAC inhibitor (Rahman et al. 2025) used to manage a variety of seizure disorders (Willmore 2003) and bipolar disorder (Bond et al. 2010; Cipriani et al. 2013); mitochondria appear more fragmented and dispersed (although the images are low-resolution), showing a positive MITO-SLOPE which is the direction expected to normalize the centralized mitochondrial localization associated with psychosis. Tolcapone, a Parkinson's disease medication, is a catechol-O-methyltransferase (COMT) inhibitor that affects dopamine levels, which is strongly linked to many psychiatric conditions. Its side effects can include hallucinations and depression (Willman & Tadi 2025).

Two drugs are known to interact with the phosphodiesterase (PDE) protein family, which has been strongly linked to psychiatric disorders (Hebb & Robertson 2007; Jiang et al. 2023) and whose inhibitors have received trials in mood and psychotic disorders, with mixed results (Delhaye & Bardoni 2021; Sadeghi et al. 2023): PF-02545920 is a PDE10a inhibitor that did not progress after Phase 2 trials in Huntington's disease (Ferguson et al. 2022) nor Phase 1b/2 trials in schizophrenia (DeMartinis et al. 2019; Walling et al. 2019), although another PDE10a inhibitor passed Phase 1 trials in Tourette syndrome (Marshall et al. 2024). Trapidil is PDE3 inhibitor and competitive inhibitor of the platelet-derived growth factor receptor (PDGFR) inhibitor that functions as a vasodilator and is subject to a patent for cognitive disorders including depression and psychosis (Bordbar 2022). Note that these PDE inhibitors have the opposite impact on mitochondrial localization; different PDEs are believed to have different impacts on psychiatric function: as noted in (Sadeghi et al. 2023), "The most promising therapeutic candidates to emerge from these preclinical studies are PDE2 and PDE4 inhibitors for depression and anxiety and PDE1 and PDE10 inhibitors for schizophrenia. Furthermore, PDE3 and 4 inhibitors have shown promising results in clinical trials in patients with depression and schizophrenia". Caffeine also targets PDEs but its effect did not reach statistical significance (d_slope = -0.45).

The MITO-SLOPE hits also included drugs without a history in psychiatric treatment, but that act by plausible mechanisms and may warrant further exploration. For example, XL-147 inhibits PI3K, a pathway considered as a target for psychiatric disorders (Y. Chen et al. 2024). Tivozanib is an inhibitor of the vascular endothelial growth factor receptor (VEGFR), a pathway with ties both to schizophrenia (Rampino et al. 2021) and depression (Wang et al. 2023). Clioquinol is an antifungal with a poorly understood mechanism of action (McKeny et al. 2025), removed from most markets due to an association with Subacute Myelo-Optic Neuropathy (Bareggi & Cornelli 2012). It has shown preclinical promise in animal studies of Alzheimer's disease (Adlard et al. 2008).

We analyzed two other public imaging datasets where compounds' impacts on mitochondrial localization could be discerned. These compound sets have far fewer annotated mechanisms of action, because they primarily contain screening compounds rather than well-studied drugs or bioactive agents. Nevertheless, we provide both lists for future studies (see Data and Code Availability). For example, these compounds could be used to train machine learning models to predict mitochondrial localization from chemical structures. In the cpg0016-jump (JUMP) dataset, we found 228 compounds meeting both criteria: statistically significant MITO-SLOPE values and fairly normal cell morphology based on the orthogonal features, but none had annotated mechanisms of action. In the cpg0012-wawer-bioactivecompoundprofiling (CDRP) dataset, we found 142 compounds as hits. Of these, only two had annotations: BRD-K28863208 (also known as PNU-282987; d_slope = -0.37), an agonist of the nicotinic cholinergic receptor encoded by *CHRNA7,* and BRD-K85242180 (-0.56), an indoleamine 2,3-dioxygenase (IDO) inhibitor also connected to nicotinic cholinergic receptors: IDO is a key enzyme in the kynurenine metabolic pathway, which has been observed to be dysregulated in both SZ and BD (Erhardt et al. 2017), and kynurenic acid modulates glutamatergic and dopaminergic neurotransmission as well as antagonizing alpha7 nicotinic cholinergic receptors (Erhardt et al. 2017; Plitman et al. 2017). Genetic associations have been observed between alpha nicotinic receptors and both SZ and BD (Thomsen et al. 2011). Smoking cigarettes, a nicotine delivery system, is common in both SZ and BD (Heffner et al. 2011; Ding & Hu 2021); nicotine is known to regulate numerous neurotransmitters and can both reduce and exacerbate mood and cognitive symptoms (Ripoll et al. 2004; Heffner et al. 2011; Ding & Hu 2021). PNU-282987 was found to reverse an amphetamine-induced gating deficit in rats (Bodnar et al. 2005) and is listed as a preclinical program for schizophrenia from Pfizer, terminated for undisclosed reasons (Gray & Roth 2007). The characteristics of these two compound hits provide some support that they produce effects relevant to the mechanisms underlying SZ or BD.

Genetic regulators of mitochondrial localization

We next virtually screened our public JUMP Cell Painting images from genetic perturbations, both overexpression (12,609 genes) and CRISPR-Cas9-mediated knockout (7,975 genes) (Chandrasekaran et al. 2024). Because no single gene determines more than a small fraction of risk for SZ or BD, we did not anticipate dramatic impacts on the mitochondrial localization phenotype, but we hoped this analysis might provide some insights and further validate the mitochondrial localization phenotype as being relevant to bipolar disorder and schizophrenia.

In the absence of true positive control genes, we took several approaches. First, although not guaranteed to impact the steady-state localization of mitochondria, we analyzed a group of genes annotated as impacting mitochondrial dynamics (fusion, fission, transport, and mitophagy) (Cuperfain et al. 2018). We found that CRISPR-Cas9-mediated transient knockout was statistically significantly enriched as lowering MITO-SLOPE (Figure 7A, less mito staining at the edge of the cell, mimicking the psychosis patient samples). The narrower mitochondrial transport category did not reach statistical significance but showed the same trend. We did not see enrichment for overexpressed genes in the same categories (Figure 7B), perhaps to be expected given that overexpression of a protein does not guarantee more

of that protein's function and generally produces less robust phenotypes in the JUMP dataset in our previous analysis (Chandrasekaran et al. 2024).

Next, we examined two particular genes associated with schizophrenia and/or bipolar disorder: The association of CACNA1C with psychotic and mood disorders is a well-replicated finding (Moon et al. 2018; Sklar et al. 2008) and GSK3B is a known target for bipolar medicines, both antipsychotics (Sutton & Rushlow 2011) and lithium (Snitow et al. 2021), with some variants associated with psychosis in some populations (Jope & Roh 2006) (though, as with most genes, it explains little of risk). We found that CRISPR knockout of CACNA1C had a dramatic pattern, matching that of major depression, while GSK3A and GSK3B had a much weaker impact (Figure 7C). We analyzed images from a public dataset from Recursion, RXRX3 (Fay et al. 2023), and confirmed the CACNA1C result while also showing a stronger result for both GSK3A and GSK3B (Figure 7D). GSK3B has a well-known role in mitochondrial activity (as reviewed in (Yang et al. 2017)), while CACNA1C has emerging evidence (Theeuwes et al. 2018; Kessi et al. 2023; Michels et al. 2018).

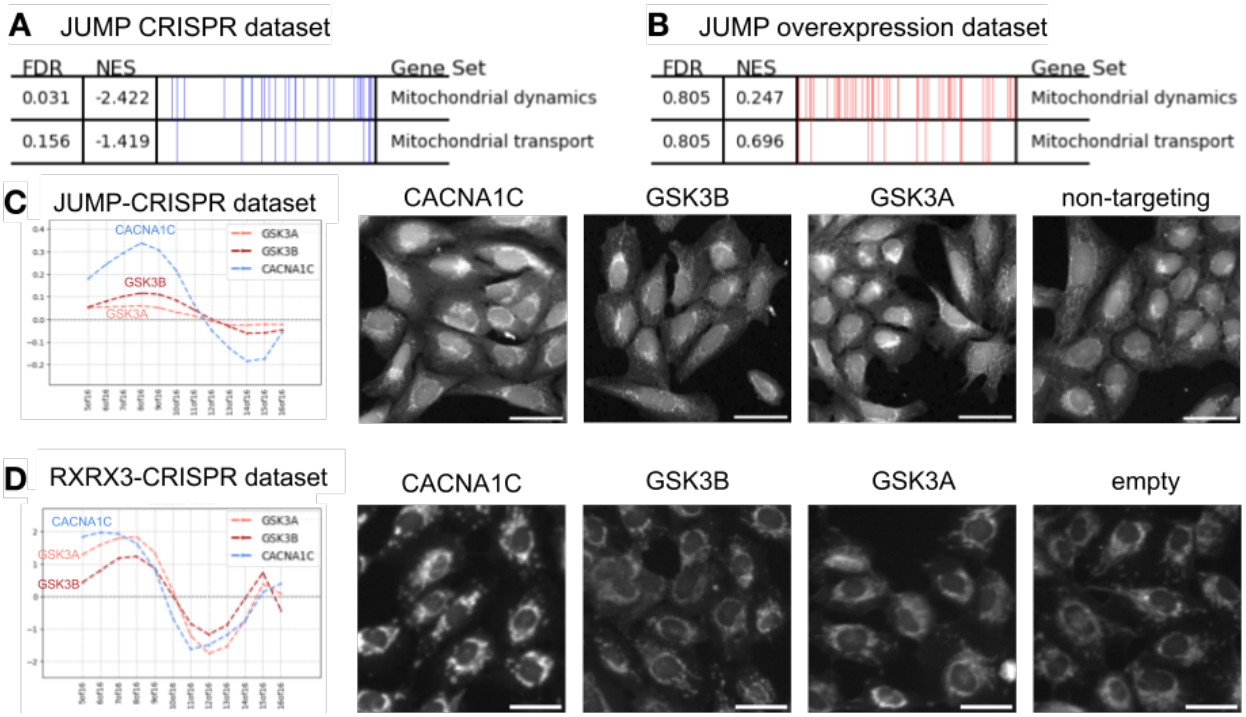

Figure 7: Mitochondrial localization impact for genes with known association with mitochondrial function or psychosis. *Mitochondrial dynamic genes are enriched for unusual MITO-SLOPE, for CRISPR knockouts (A) but not overexpressed genes (B); mitochondrial transport genes are not significantly enriched in either dataset. The vertical lines in each row represent the positions of individual genes from that functional category within the ranked list of all genes ordered by MITO-SLOPE values. Gene annotations are taken from Cuperfain, et al., Table 3 (Cuperfain et al. 2018). FDR and NES are as defined in Figure 5. (C and D): As calculated from images in the JUMP-CRISPR dataset of U2-OS cells (C) or RXRX3-CRISPR dataset of Human Umbilical Vein Endothelial Cells - HUVEC (D), we show the distribution of mitochondria in bins from the nucleus (left) to cell edge*

(right), as in Figure 4B (which shows the patterns of each patient category; all 3 genes here show a similar pattern as seen in patients with major depression). Right: Example images from each gene alongside negative controls; an image was selected at random for each condition, cropped to regions with similar cell density representative of the whole image, and scaled similarly for visibility. Both JUMP and RXRX3 datasets contain multiple other channels of stained cellular compartments (shown in Supplementary Figure 6); the RNA channel was used to segment the cell borders during image analysis. Scalebar = 50 µm.

Finally, we analyzed the full list of gene perturbations in both JUMP datasets, to identify those that most strongly produced the psychosis-associated mitochondrial phenotype (Figure 8). Three genes met the criteria for their CRISPR-Cas9-mediated knockout impacting MITO-SLOPE without markedly impacting non-mitochondrial-related features: *SP1*, *TBX3*, and *KCNH6* (Figure 8A). Of note, CACNA1C was at the ~4th percentile but impacted other features. This highlights a tradeoff in our filtering strategy: some genes with known psychiatric associations were excluded to ensure specificity; all data is publicly available in case researchers would prefer to use a more lenient orthogonal features filter. SP1 is a transcription factor regulating genes involved in many cellular processes, including mitochondrial transcription factors A and B (TFAM, TFB1M and TFB2M) in neurons (Dhar et al. 2013). SP1 has a strong connection with schizophrenia as reviewed in the introduction of Pinacho, et al., which itself found that *SP1* mRNA expression is significantly increased in the hippocampus in patients with chronic schizophrenia in post-mortem samples (Pinacho et al. 2014). SP1 is also associated with autism (Thanseem et al. 2012) and Alzheimer's disease (Citron et al. 2008; Santpere et al. 2006). Particularly interesting is that SP1 regulates the expression of *TBX3*, the second-most significant gene on the list (Smith et al. 2011). TBX3 is another transcription factor, regulating developmental processes including in hypothalamic neurons (Shi et al. 2022), but without strong links to psychiatric illness. The third hit, *KCNH6*, is a potassium channel subunit that modulates cardiac repolarization and heart rate, as well as neuronal excitability, with some links to mitochondrial health. For example, it "enhances hepatic glucose metabolism by regulating mitochondrial Ca2+ levels and inhibiting oxidative stress" (Zhang et al. 2022) and is located in mitochondria and impacts mitochondrial metabolism (Han et al. 2025) and function (Zhao et al. 2023). Most of the seven genes just below the threshold of significance (RHOU, POLE3, DRD1, KCNA1, FARS2, FOXQ1, ASCL1) have roles in mitochondrial function or psychiatric conditions as well.

A Mitochondrial mislocalized genes: CRISPR-Cas9 knockout

Gene symbol	Gene name	d_slope (mito)	p_orth_ std (other)	mean cell count	JCP2022 ID	NCBI Gene ID
SP1	Sp1 transcription factor	0.79	0.09	390	JCP2022_806714	6667
TBX3	T-box transcription factor 3	0.71	0.05	456	JCP2022_806979	6926
KCNH6	potassium voltage-gated channel subfamily H member 6	0.66	0.18	459	JCP2022_803582	81033

B Mitochondrial mislocalized genes: overexpression

Gene symbol	Gene name	d_slope (mito)	p_orth_ std (other)	mean cell count	JCP2022 ID	NCBI Gene ID
CDK18	cyclin dependent kinase 18	-1.05	0.06	129	JCP2022_909732	5129
MARK3	microtubule affinity regulating kinase 3	-0.81	0.07	113	JCP2022_906141	4140
SHC1	SHC adaptor protein 1	-0.70	0.09	132	JCP2022_901430	6464
DCTN4	dynactin subunit 4	-0.69	0.12	129	JCP2022_907704	51164
IHH	Indian hedgehog signaling molecule	-0.67	0.05	122	JCP2022_910178	3549
DNAJC22	DnaJ heat shock protein family (Hsp40) r	-0.64	0.06	122	JCP2022_903892	79962
ATOH7	atonal bHLH transcription factor 7	-0.62	0.12	116	JCP2022_914296	220202
SCAMP4	secretory carrier membrane protein 4	-0.62	0.05	114	JCP2022_904347	113178
EDA2R	ectodysplasin A2 receptor	-0.53	0.13	125	JCP2022_903646	60401
PNLIP	pancreatic lipase	-0.52	0.65	124	JCP2022_901153	5406
KLHDC3	kelch domain containing 3	-0.46	0.06	132	JCP2022_913401	116138
DELE1	DAP3 binding cell death enhancer 1	-0.44	0.07	124	JCP2022_907005	9812
MFAP3	microfibril associated protein 3	-0.41	0.14	126	JCP2022_906157	4238
PSG2	pregnancy specific beta-1-glycoprotein 2	-0.40	0.28	116	JCP2022_912990	5670
ZNF277	zinc finger protein 277	0.47	0.07	103	JCP2022_910821	11179
NT5E	5'-nucleotidase ecto	0.53	0.04	116	JCP2022_910257	4907
SHPK	sedoheptulokinase	0.54	0.23	117	JCP2022_914043	23729
CEP70	centrosomal protein 70	0.55	0.40	160	JCP2022_911835	80321
LSM14B	LSM family member 14B	0.55	0.16	123	JCP2022_912355	149986
POC5	POC5 centriolar protein	0.55	0.04	138	JCP2022_904579	134359
DCUN1D4	defective in cullin neddylation 1 domain	0.58	0.09	145	JCP2022_910893	23142
P3H2	prolyl 3-hydroxylase 2	0.59	0.10	104	JCP2022_913242	55214
TMEM91	transmembrane protein 91	0.60	0.24	153	JCP2022_909483	641649
MECOM	MDS1 and EVI1 complex locus	0.63	0.08	112	JCP2022_910076	2122
H2AC1	H2A clustered histone 1	0.65	0.05	111	JCP2022_904919	221613
TSPAN10	tetraspanin 10	0.66	0.49	131	JCP2022_908524	83882
SLC25A35	solute carrier family 25 member 35	0.69	0.06	136	JCP2022_905263	399512
WDFY3	WD repeat and FYVE domain containing	0.73	0.07	105	JCP2022_914728	23001
ASPRV1	aspartic peptidase retroviral like 1	0.73	0.19	130	JCP2022_912374	151516
TP53RK	TP53 regulating kinase	0.76	0.06	121	JCP2022_904339	112858
PFKL	phosphofructokinase, liver type	0.77	0.08	133	JCP2022_909780	5211
FHL1	four and a half LIM domains 1	0.80	0.06	101	JCP2022_900531	2273
CIDEA	cell death inducing DFFA like effector a	0.81	0.12	110	JCP2022_909518	1149
CCDC102B	coiled-coil domain containing 102B	0.82	0.24	123	JCP2022_911775	79839
MAPK9	mitogen-activated protein kinase 9	0.85	0.15	103	JCP2022_913829	5601
PIK3CB	phosphatidylinositol-4,5-bisphosphate 3	0.87	0.07	123	JCP2022_901125	5291
CNOT3	CCR4-NOT transcription complex subuni	0.89	0.09	82	JCP2022_906222	4849
ETS2	ETS proto-oncogene 2, transcription fact	0.92	0.10	87	JCP2022_914411	2114
RHOBTB2	Rho related BTB domain containing 2	0.93	0.07	121	JCP2022_907342	23221

Figure 8: Exploration of genetic hits in virtual screen. *The tables show genes that increase (blue) or decrease (red) mitochondria towards the edge of the cells as measured by d_slope (as described in Figure 6) in the two datasets (A) JUMP-CRISPR and (B) JUMP-overexpression. p_orth_std is used as an additional filter, measuring whether non-mitochondrial-related features were significantly different from controls*

- to ensure the remainder of cell morphology remained fairly normal (see Methods). The hits do not dramatically impact cell count, as shown.

The 39 hits in the overexpression data were not all clearly linked to mitochondrial function or psychiatric conditions; many are linked to cancer, indicating that they may be more related to changes in overall cell shape, despite the filter we applied to exclude major changes in orthogonal features. Enrichment analysis failed to find consistent known annotations among the hits, apart from some growth and cancer related categories around $p \sim 0.05$ (Supplementary Figure 7). Nevertheless, among the 14 negative slope hits, we found DELE1, a mitochondrial-localized protein involved in mitochondrial stress response (Fessler et al. 2020), which is itself linked to mood and psychotic disorders (see Introduction). Two genes relate to intracellular transport: DCTN4 (Dynactin Subunit 4) is "part of the dynactin complex that activates the molecular motor dynein for ultra-processive transport along microtubules" (GeneCards Human Gene Database n.d.) and MARK3 (microtubule affinity-regulating kinase 3) regulates microtubule stability (Drewes et al. 1997). These functions can impact proper trafficking of mitochondria in axons, which is also linked to CNS disorders (Zheng et al. 2019); for instance, inhibiting dynactin components genetically in Drosophila yielded defective axonal transport of mitochondria (Pilling et al. 2006; Saxton & Hollenbeck 2012). EDA2R was found as a biomarker associated with lower cognitive ability and brain volume in human aging (Harris et al. 2020). MFAP3 has been reported as a biomarker for pain (Niculescu et al. 2019). Three negative-slope hits have no reported linkage to little direct linkage to mitochondrial positioning or psychiatric conditions but are otherwise related to mitochondria: CDK18, is a cyclin-dependent kinase located in mitochondria and involved in myelination (Anon n.d.). Isoforms of SHC1 are scaffolding proteins that target the mitochondrial matrix and affect mitochondrial associations with other cellular elements (Anon n.d.). ATOH7 is a transcription factor and is associated with regulation of mitochondrial activity in retinal cell development ((Brodier et al. 2020). For the remaining six hits, we found no evidence reported for direct linkage to mitochondrial positioning or psychiatric conditions (IHH, coding for several hedgehog signaling molecules; DNAJC22, a heat shock related molecular chaperone; SCAMP4, an integral membrane carrier protein; PNLIP, a pancreatic triglyceride lipase; KLHDC3, involved in ubiquitination; and PSG2, in the immunoglobulin family related to cell adhesion).

The 25 positive-slope JUMP-ORF genes also include cancer-related genes regulating growth and differentiation. Still, there are many other genes related to psychiatric conditions and/or mitochondrial function. WDFY3 (WD repeat and FYVE domain containing 3, also called ALFY) is involved in vesicle trafficking and membrane dynamics, especially autophagy, including mitophagy (Napoli et al. 2021). It is highly expressed in the central nervous system and disruption of the Drosophila homolog, bchs, disrupts axonal transport of endolysosomal vesicles (Lim & Kraut 2009) and yields brain degeneration (Finley et al. 2003). In humans, WDFY3 is a genetic risk factor for intellectual and developmental disabilities (IDD), microcephaly and neuropsychiatric disorders including schizophrenia, as reviewed in (Dragich et al. 2016). Several other hits are implicated in autophagy, such as CIDEA and TMEM91's family members, and mitochondrial function, such as SHPK (Franceschi et al. 2022) and SLC25A35, a mitochondrial Solute Carrier Family 25 protein family member

widely expressed in the CNS (Haitina et al. 2006). CIDEA also transcriptionally regulates UCP1 (Mitochondrial Brown Fat Uncoupling Protein 1) which is also a Solute Carrier Family 25 Member (Jash et al. 2019). Other hits have associations to neurodevelopmental disorders, including RHOBTB2 (Langhammer et al. 2023) mutant forms of which can accumulate in mitochondria and disrupt form and function (Miyamoto et al. 2025) and CNOT3 (Martin et al. 2019), which stabilizes mRNAs involved in mitochondrial function (Suzuki et al. 2015). Finally, ETS2 was identified as the causal gene for a non-coding variant in chromosome 21q22 (Stankey et al. 2024) that promotes a mitochondrial death pathway (Helguera et al. 2005). 21q22 is associated with Down's Syndrome, which is associated with increased psychiatric/psychosis risk (Rivelli et al. 2022).

Discussion

As reviewed in the introduction, the connection between mitochondrial structure/function and psychotic disorders is well-established from multiple streams of evidence. Here, we found in a cohort of 168 patients that those experiencing psychosis showed mitochondria less localized at the edge of fibroblasts. By querying existing large chemical and genetic perturbation datasets in cancer cell lines, we found that many genes and compounds that impact mitochondrial localization are implicated in brain function and psychiatric conditions.

Transport of mitochondria is tightly regulated and linked to human disorders (Mandal & Drerup 2019). Although the specific phenotype we observed, sometimes called perinuclear mitochondrial clustering, is relatively poorly understood, it may be associated with several other disorders (Al-Mehdi et al. 2012). The aberrant transport of mitochondria has been linked to schizophrenia and bipolar disorder via several lines of evidence (Flippo & Strack 2017; Scaini et al. 2021). For example, the gene DISC1, Disrupted in Schizophrenia 1, is linked to schizophrenia, depression, bipolar disorder and autism (Murphy & Millar 2017), and mitochondrial dynamics in neurons were impacted by altering DISC1 levels (Atkin et al. 2011) and by large aggregates of DISC1 (Atkin et al. 2012). Mood stabilizers were found to impact proteins involved in mitochondrial transport in synaptoneurosomal preparations from rat pre-frontal cortex (Corena-McLeod et al. 2013). The *C. elegans* protein ANC-1, homolog of human genes (SYNE1/2) associated with various neuropsychiatric conditions, was found to promote localization of mitochondria to the base of the proximal axon (Fischer et al. 2022). Knockout of the schizophrenia-associated protein dysbindin yielded a significant decrease in mitochondrial density in distal axons, which impaired calcium dynamics (Suh et al. 2021). Together with our prior findings including autopsied brain (Cataldo et al. 2010), we believe there is sufficient evidence that the mitochondrial localization phenotype we observe in human patient fibroblasts here is also found in other brain-relevant cell types and in physiological structures *in vivo*.

We can only speculate as to the mechanism by which mitochondrial localization might impact neuron function and ultimately brain function. A recent study found that rather than producing ATP as is typical in most contexts, axonal mitochondria in cortical pyramidal neurons in mice actually consume ATP (Hirabayashi et al. 2024); this builds upon prior work showing that presynaptic release sites lacking mitochondria have a higher likelihood of

neurotransmitter release than those with mitochondria (Kwon et al. 2016; Vaccaro et al. 2017). Our findings may be consistent with this: the lack of mitochondrial transport away from the nucleus that we observed here would imply that in psychosis, fewer mitochondria result in more ATP/energy being available in axons, reducing barriers to neurons firing. However, mitochondria produce numerous substrates necessary for cell function, including neurotransmission. These substrates may be lacking in terminals with lower levels of mitochondria. As well, changes in cytoskeletal structure, often involving microtubules, are well-documented in various cell types of patients with bipolar disorder and schizophrenia (Marchisella et al. 2016; Benítez-King et al. 2016; Snelleksz & Dean 2021; Brown et al. 2014). Because some genes associated with bipolar disorders and schizophrenias are also associated with the microtubular cytoskeleton (Perrottelli et al. n.d.), drugs targeting this cytoskeleton have been proposed as potentially therapeutic for psychotic and other brain disorders (Varidaki et al. 2018). These processes may also impact mitochondrial localization.

This study has several important limitations. First, because of the challenges of obtaining consented patient samples and growing multiple patient cell samples, our cohort is limited to 168, spread across the conditions tested, and was collected in one clinical location with subjective diagnostic annotation. Still, this is larger than most cohorts published for other disorders and offers some mitigation of concerns about donor variability due factors such as genetics, sex, age, and comorbidities. Second, it is virtually impossible to obtain samples from patients who are untreated with medications, and most patients are on multiple medicines of varying mechanisms. Although the phenotypes we observe are those that persist in cells cultured through several passages and media changes and across patients taking different classes of medicines, we cannot rule out impacts by drugs the patients had been taking. Likewise, we cannot control for other unrecorded factors associated with these conditions, such as diet and exercise. Third, the study assessed a single cell type from patients, fibroblasts, because they are readily obtainable and robust in culture. As noted in the introduction, this strategy has been successful for other brain disorders, and other transport mechanisms have been found consistent across many cell types (Goering et al. 2023). Nevertheless, we have begun to explore mitochondrial localization in more physiologically relevant brain cells, specifically astrocytes derived from the fibroblasts used in the studies reported here - preliminary results show altered mitochondrial localization consistent with that reported in this study; such reprogramming of the fibroblasts to induced pluripotent stem cells (iPSC) followed by induced differentiation to astrocytes is time-consuming but also has the advantage of resetting most epigenetic marks, thus reducing concerns about medication exposure or other environmental differences between patients and controls. Fourth, we report our observations but do not explore the mechanisms underlying the changes in MITO-SLOPE observed: MITO-SLOPE captures mitochondrial localization, which is itself influenced by the intensity of MitoTracker staining, which is influenced by mitochondrial membrane potential - it therefore combines spatial and intensity information, such that disentangling localization from mitochondrial membrane potential is not completely possible. In fact, we believe that the patient phenotype likely reflects multiple cellular changes beyond mitochondrial distribution, including cytoskeletal alterations documented in prior studies. And fifth, we performed virtual screening only, no experimental validation of chemical or genetic hits was conducted in patient-derived cells.

Finally, the use of this mitochondrial phenotype as a platform for drug discovery should be approached with caution, as we have previously noted more generally (Chandrasekaran et al. 2020). Most screening strategies that translate findings from cell culture to the human organism are subject to caution; reversing disease-associated phenotypes poses some additional pitfalls. For instance, disease-associated phenotypes may reflect correlation with the patients' problematic symptoms and not causation. In such cases, drugs reversing the phenotype may be ineffective or "even worse, the detected phenotype might reflect the cells' attempt to mitigate the impact of the disease perturbation, such that drugs reversing the phenotype would aggravate the condition in patients" (Chandrasekaran et al. 2020). That is, the observed phenotype may be a useful compensation for the abnormalities underlying illness. In that case, reversing the compensation would be anti-therapeutic, although given the tentative observation here of a spectrum of localization with psychosis on one end and depression on the other, medicines at either end might prove useful.

We found that several existing classes of medications used to treat psychosis were not associated with mitochondrial mislocalization. Optimistically, the mitochondrial localization phenotype could represent a novel mechanism by which psychosis might be remedied and is therefore worthy of future chemical screening. Still, there are several reasons why drugs that treat these conditions may not reverse the mitochondrial phenotype in patient fibroblasts nor cancer cell lines. Potential alternative explanations include: (a) the cell type (whether the cancer cell line used in public datasets stained for mitochondria studied here, or a particular patient's fibroblasts that might be used in a future screen) might be missing key components necessary for proper response, especially the targets of the given drugs. Given that drugs do not work equally well across patients, we would expect heterogeneity in assay response as well, so a future screen would ideally test multiple patient cell lines. As noted earlier, testing more brain-relevant cell types would be ideal, albeit costly, though this may not be necessary for a primary drug screen for compounds working by this mitochondrial localization mechanism. (b) The timing may not be appropriate; existing psychiatric medications typically take 2-3 weeks to show relief of symptoms in patients, although it is also possible that this is only the case due to the complexity of full organ systems. (c) Drug metabolic processes that are only functional in the whole organism may be necessary for the impact of effective drugs in this context. (d) Drug dose, although tested across a range, may be unsuitable.

Future studies could evaluate the genes and compounds we identified for their impact on mitochondrial localization directly in a collection of patient cell lines, whether fibroblasts or iPSC-derived neural cells, to confirm mitochondrial phenotype reversal and evaluate generalizability (potentially across all 168 cell lines, and/or using reprogrammed/differentiated brain cell types derived from them). Multiple readouts of mitochondrial and cytoskeletal structure and function could be evaluated beyond MITO-SLOPE, including posttranslational modifications, mitochondrial transport speed and pausing frequency, membrane potential, and integrity of the microtubular network. It could also be valuable, albeit expensive, to physically screen compounds to find those impacting mitochondrial localization in fibroblasts from patients experiencing psychosis, rather than this study's virtual query in unaffected patients' cancer cell lines. In such a setting, where images are collected in a single well-controlled experiment, searching for compounds that

reverse a machine-learning based disease phenotype is more feasible, rather than the single feature used here to facilitate virtual screening using publicly available data.

Overall, we found here that the mitochondrial phenotype we originally observed in a small cohort of bipolar patient fibroblasts and which was seen in our prior study of post mortem brain, is now consistently observed across a much larger group of patients experiencing the most common conditions associated with psychosis. We find this phenotype is induced by perturbation of genes associated with these conditions, and is influenced by drugs that impact pathways known to influence symptoms in human patients. Given the strong evidence in the literature for mitochondrial function disruption in these diseases, and given that the phenotype could be simplified to a single feature, the mitochondrial dispersion phenotype appears to be well suited for further virtual and physical screening to identify novel targets and therapeutic candidates.

Methods

The protocol for cell culture, sample preparation, and imaging is described in Methods but also provided online (https://github.com/carpenter-singh-lab/2024_Haghighi_Mito/blob/main/McleanCollectionFibroblastGrowthProtocol.md).

Primary cell lines

Fibroblasts were derived as in (McPhie et al. 2018). All subjects provided written informed consent, as approved by the McLean Hospital/Mass General Brigham (formerly Partners Healthcare) Institutional Review Board IRB# 2007P002597.

Human fibroblast cell lines were grown as in our prior study (Cataldo et al. 2010). Three passages were done prior to plating onto glass coverslips for staining and imaging. Cells were plated at a density of 7.9 x 10^3 cells per cm^2. MitoTracker-M7510, 125 nmol/L (Invitrogen Corporation, Carlsbad, CA), was used to visualize mitochondria according to manufacturer's instructions, with a 30 minute live incubation. Cytoskeletal integrity was examined by immunocytochemistry using Phalloidin-488 (1:500) according to the manufacturer's protocol and nuclei were visualized by Hoechst 33342 trihydrochloride (2 ug/ml). Two coverslips per line were mounted in Fluoro-Gel aqueous mounting media (Electron Microscopy Sciences, Hatfield, PA).

Imaging

For each patient sample, fifty fields were selected manually and imaged at 400X in three independent channels on a Zeiss Axiovert Observer 2.1 with a Colibri 2 LED illumination system. Image acquisition was done with Zeiss Zen 2.0 software using consistent imaging settings from condition to condition, including exposure times - for example, channel settings: DAPI 40 ms/40%, brightness, offset -0.80 um. Green 400 ms/50% brightness. Red 800 ms/100% brightness. Single channel images were exported as high resolution TIFF files as both color and black and white images as well as one merged three-color image. Images were visually checked for focus, defined edges on each cellular element to be analyzed. Cells

with nuclei touching the border of the image are excluded from analysis by the automated pipeline. Image fields of view were selected to avoid regions where cells significantly overlapped/grew on top of each other. Images had median 8.5 +- 2.2 (stdev) cells in them showing that they had a consistent number of cells. Overall, segmentation quality was good, for primary fibroblasts.

For visualization in Figure 2, each fluorescence channel is independently normalized by its maximum intensity and contrast-enhanced by clipping to the 0.5th–99.5th percentiles, then rescaled to 8-bit (0–255). The composite image is generated by averaging the colorized channels and rescaling to 0–255. The final column shows grayscale crops from the mitochondrial channel after per-image max normalization but without additional percentile clipping. All intensity adjustments are applied for visualization only, as absolute staining intensity is not the phenotype of interest in this figure.

Image analysis and feature engineering

A set of images, obtained as described above, of nuclei, cytoskeleton, and mitochondria were processed by an image analysis pipeline to quantify the mitochondria within individual cells using CellProfiler 3 (McQuin et al. 2018) or CellProfiler 4 (Stirling et al. 2021). The nucleus was segmented using a seed-based watershed algorithm on DAPI images. The cell objects were seeded from nuclei objects and were segmented on actin images or on mitochondria images and then expanded to actin images. We also applied filters to remove cells touching the border, with segmentation issues, and with intensity artifacts as described in the Github repository for the project. The CellProfiler pipelines for processing fibroblast data are available at the project's github repo and contain detailed parameters; here we describe each step of this pipeline for the patient fibroblast cohort:

1) **LoadData:** Single-channel grayscale images are loaded for DAPI (Hoechst), Phalloidin488 and MitoTracker (m7510) channels. Relevant Metadata and Groups are set.
2) **IdentifyPrimaryObjects**: This step segments the stained nuclei. To aid correct segmentation of the nuclei as objects, objects are excluded based on extreme size, and based on touching the edge of the image. An automatic declumping algorithm is applied in this step to separate adjacent nuclei.
3) **IdentifySecondaryObjects:** A two-step strategy is used to identify the cell edge. First, the mitochondrial network image is used to get close to the outer edge of the cell and this is called the "precell"; this is helpful for cells that do not have strong actin staining throughout the cytoplasm. Then, the actin image is used to get the correct segmentation starting from the edge of the precell all the way to the outer cell edge.
4) **IdentifyTertiaryObjects:** This step segments the "cytoplasm" objects by subtracting the Nuclei object from the Cells object.

A series of measures are then done on the segmented objects: The idea is to measure a large number of parameters that will be used in the unbiased machine learning analysis to determine where the largest differences are seen between the groups.

5) **MeasureColocalization**: This module applies various algorithms measuring co-localization within the segmented objects.

6) **MeasureGranularity:** This module allows granularity to be measured within the segmented objects. Granularity is a texture measurement that tries to fit a series of structure elements of increasing size into the texture of the image and outputs a spectrum of measures based on how well they fit.
7) **MeasureObjectIntensity:** This module measures a number of intensity features for segmented objects.
8-10) **MeasureObjectNeighbors:** These three modules quantify spatial relationships between objects of interest.
11) **MeasureObjectIntensityDistribution:** This module measures the spatial distribution of intensities within an object using concentric annuli (rings) from a designated point. At this point of the pipeline, this step is done considering the identify primary, secondary and tertiary objects.
12) **MeasureObjectSizeShape:** This module measures many area and shape features (area, perimeter and others) of segmented objects.
13) **MeasureTexture:** This module measures the roughness or smoothness of the staining in an object by measuring the intensity variations in their grayscale images.
14) **EnhanceOrSuppressFeatures:** This module enhances or suppresses the intensity of certain pixels relative to the rest of the image, by applying image processing filters to the image. It is used in this pipeline to enhance the staining of the mitochondrial network so that the overall spatial distribution of the mitochondrial staining can be identified and then measured in a later step. It uses a tubeness filter (algorithm) that enhances filamentous (neurite like) structures of a specified thickness (https://www.longair.net/edinburgh/imagej/tubeness) (Sato et al. 1998). At the end of this module the tubeness image is intensity-rescaled. In essence, this module generates a compromise between the original intensity image and a segmented image. Its purpose is to sharpen the intensity staining without completely turning it into a binary image.
15) **Threshold:** A threshold filter is then applied to the tubeness image in order to determine what intensities are considered foreground and background; this is used in the next module.
16) **MorphologicalSkeleton:** Creates a skeleton from the thresholded mito tubeness image. It delineates the area of the image to be measured in the next module.
17) **MeasureObjectSkeleton:** This module measures the number of trunks and branches for each branching system in an image. The module takes a skeletonized image of the object plus previously identified seed objects and can generate measures of the complexity of the branching object, in this case the contiguous parts of the mitochondrial network.
18-20) **ImageMath:** This module is used to do simple mathematical operations on image intensities. It can also be used without performing a mathematical operation to simply duplicate an image for renaming to be used in a downstream operation. This latter function is what it is used for at this step of the pipeline in order to have three independent image names for the three types of radial distribution measurements in the three MeasureObjectIntensityDistribution modules.
21-23) **MeasureObjectIntensityDistribution:** The mitochondrial pipeline uses three MeasureObjectIntensityDistribution steps. Each measures the radial distribution of the enhanced mito tubeness image in concentric annuli (rings). They differ by where the inner edge (center) of the first annuli is set. For the patient fibroblast images, the inner

edge of the annuli is set at the outer edge of the nucleus (CEN). The other modules were used with images from the other cell types. MITO-SLOPE uses the series of measurements made by this module.

23) **MeasureImageIntensity:** This module measures the intensity of the whole image and the intensity of the background, in regions without cells.

24-25) **OverlayOutlines:** This module overlays an outline of an area of interest on an original of other type of segmented image that is in the pipeline. It allows one to go back and check that the areas measured at different steps correspond to the areas of interest in the original images.

26-27) **Save images:** At this point in the pipeline this module saves an image of the outline created in OverlayOutlines step on an earlier image from the pipeline.

28) **ExportToSpreadsheet**: Data (Measurements) are exported as .csv files for further analysis.

For displaying the example hit images for the LINCS dataset, intensities were rescaled relatively, for visualization, as follows: the MitoTracker image is raised to power of 0.4 then rescaled to the min/max for each image. Then, the red-green-blue merged image is made with MitoTracker and DNA as red and blue, respectively, and rescaled with a set range of .05-.7. Finally, cell outlines from CellProfiler are overlaid in white.

Patient group classification using machine learning

We performed patient category classification for various psychosis spectrum subgroups versus control using the patient-level morphological representations. Each patient has a bag of single cell samples and we form per-bag representations as the median of single cell samples representations in each bag when training a traditional ML classifier. We used a subset of mitochondria channel features extracted by CellProfiler for learning a logistic regression classifier. We used raw single cell mitochondria channel images for learning a CNN deep learning based classifier and we evaluated performance of each learned model through stratified K-fold cross validation (K=10). The area under the receiver operating characteristic curve (AUC-ROC) is reported for each binary classification as the measure of classification performance.

CellProfiler features extracted from the mitochondria channel form a set of 326 highly correlated features. This multicollinearity in our data could affect the feature importance exploration analysis. We handled multicollinearity in our data by forming subgroups of highly correlated features and selecting one feature from each cluster as the feature selection criteria. Subgroups of features were formed by application of hierarchical clustering on Pearson correlation of features and median of each cluster was selected as the representative feature for each subgroup. Supplementary Figure 8 shows the clustering dendrogram and feature subgroups. Y-axis threshold for forming clusters was selected to form a maximum number of clusters while keeping a Variance Inflation Factor (VIF) less than 10 for each feature in the final set. This resulted in a set of 45 representative features used for feature importance exploratory analysis. We note that while using this representative set degrades the classification performance results, it was a necessary step for feature interpretation analysis which is crucial in this study. Classification results reported in Figure 3 consider all of the set of mitochondrial features, however the feature importance analysis

was based on the models learned from the representative set of features (Supplementary Figure 9). This analysis examined only the patient categories that had an AUC-ROC > 0.6 even after using the representative set of features for classification. Features with an AUC-ROC< 0.6 were considered to be indistinguishable from the Control class based on this analysis.

Feature interpretation and design of the MITO-SLOPE metric

In our effort to select a metric for virtual screening, we considered many factors in addition to the power to distinguish patients experiencing psychosis. We wanted the metric to not involve combining multiple features, which requires choices about their relative normalization and balance. We wanted a feature that could be robustly measured across datasets, especially the public datasets we planned to use for screening, which are lower resolution than our patient fibroblast study.

To make this choice, we began by examining the 45 representative features from the Feature importance analysis, in the context of our knowledge of image analysis and our visual observations over the years for cells across these psychiatric conditions. This analysis is based on the logistic regression model's coefficients and permutation importance; the top ten features from this analysis are reported in Supplementary Figure 9. Model coefficients and permutation importance results reveal that the following categories of features had the most distinctive power across various patient categories versus control samples:

(a) A subset of texture measures in the nuclei and cytoplasm area of the mito channel.
(b) A subset of features measuring the area of the image covered by mitochondria in concentric rings across the cell. These features capture the spatial patterns of the mitochondrial network across the cell and the potential shifts of this network toward the nucleus center or edge.

We therefore chose to calculate MITO-SLOPE on a single series of measured features in category (b): Cells_RadialDistribution_MeanFrac_mito_tubenessXof12 (CEN), where X ranges from 1 to 12. MITO-SLOPE is fundamentally a localization metric that quantifies the gradient of change in mitochondrial network density towards the cell edge. Figure 4A shows this pattern from the nucleus edge to the cell edge across 12 rings defined in the cytoplasm area of a cell. The promise of this metric lies in its adaptability to cell size, cell-to-nuclei size ratio, cell segmentation errors, staining intensity, image resolution, and other sources of batch-to-batch and cross-dataset variations. Also, it is not impacted by changes that occur to mitochondria upon certain fixation techniques (Whelan & Bell 2015). MITO-SLOPE measures the slope of the change in the normalized intensity values in each bin, focusing on the final bins close to the cell edge. In some public datasets in this study, the bins defined for extracting features either start from the cell center (C for "Cell" for LINCS dataset) or from the nuclei center (CCN for "Cell from Center of Nucleus" for the rest of genetic or chemical datasets) rather than from the nucleus edge (CEN for "Cell from Edge of Nucleus"). Therefore capturing the pattern at the final bins makes the pattern more transferable across datasets used for virtual screening. "Final" here is defined below ("last extremum").

MITO-SLOPE is negative for psychosis (less mito at edge) so potential drugs should yield positive MITO-SLOPE. MITO-SLOPE is positive for depression (more mito at edge) so potential drugs should yield negative MITO-SLOPE.

Algorithm for calculation of MITO-SLOPE

Inputs:

- A table containing single cell profiles of all the population with mito_tubeness radial-distribution columns for MeanFrac across all radial bins. Radial bins are the 12 rings ordered from nucleus edge to cell edge (indices: RING-11 … RING).
- Labels for each cell ("Control" vs. patient groups).

Output:

- **MITO-SLOPE** (a scalar per subject).

STEPS:

1. **Column-wise standardization (z-scoring)**
   Standardize each feature so that each column of the table has mean 0 and SD 1. All subsequent steps use these z-scored values.

2. **Per-subject aggregation (MeanFrac)**
   For each subject, average the z-scored MeanFrac radial-bin columns across that subject's cells to obtain a per-subject profile; $I_{subject}[i]$ for i = 0 … B−1 (B = 12).

3. **Control mean profile**
   Compute the mean profile across all Control subjects; $I_{control-mean}[i]$

4. **Control differencing**
   For each subject, form $\Delta I[i] = I_{subject}[i] - I_{control-mean}[i]$

5. **Smoothing**
   If desired (required on datasets with noisy measurements), apply a light 1D smoothing to ΔI. (we applied a Savitzky–Golay filter to ΔI using window_length = 5 and polyorder = 3 (length preserved). This reduces noise while retaining local trends.)

6. **Last extremum**
   Find the positions of the global maximum and global minimum of ΔI.
   Restrict to indices 0 … B−3 (exclude last 2 bins prone to segmentation errors); if neither extremum lies in this range, set MITO-SLOPE = 0 (no valid last extremum).

Otherwise, take the later (rightmost) of the two extremum positions within 0 … B−3 as the "last extremum."

7. **Slope to the edge**
   Compute **MITO-SLOPE** as:

$$\text{MITO-SLOPE} = \frac{\Delta I\,[B-1] - \Delta I[last\ extremum]}{(B-1) - (last\ extremum)}$$

Units: z-score change per bin.

Interpretation:
• MITO-SLOPE > 0 → peripheral enrichment of mitochondrial signal relative to controls.
• MITO-SLOPE < 0 → central shift relative to controls.

Analysis for virtual screens of chemical and genetic perturbation datasets

We perform the following data processing and analysis on each of the chemical and genetic perturbation datasets to obtain a ranked list of perturbations that modulate the target metric corresponding to mitochondrial dispersion relative to its untreated or control state.

We form a set of features based on patient fibroblast data that have weak linear correlation with the target metric (filtering to less than a 0.3 absolute correlation coefficient with the target metric) and are also not distinctive across various groups of patients versus the control group (filtering to less than a certain threshold defined on the mutual information between the features and the class labels). We decrease redundancy in the set by reducing the features so that those in the filtered set have less than a 0.8 correlation coefficient with each other. We call this the *orthogonal* set of features and use it as a control set of features in which minimal variability is desired. This means we do not want the genetic or chemical perturbations to dramatically change the other dimensions of cell morphology while modulating MITO-SLOPE. The threshold p-value is set based on multiple hypothesis-corrected (adjusted) p-values that therefore differ across datasets. The values of target_bh_corrected_critical_dict were:
{'taorf': 0.00409,
'lincs': 0.00761,
'CDRP': 0.00924,
'jump_orf': 0.00198,
'jump_crispr': 0.007,
'jump_compound': 0.00365}

Note that while the extracted morphological feature sets are almost consistent across various chemical and genetic datasets, the set of features and channels in patient fibroblast data differ from those in the perturbation datasets. We derive the orthogonal set based on the fibroblast dataset and based on the overlap of those features with those available in the

other datasets. As well, during revision we re-examined all patient annotations and as a result reclassified subject 272 and MCL004; this did not impact conclusions of the paper and given the minimal impact of the reclassification on orthogonal features, we kept the original version of them for simplicity.

Perturbation datasets are described in the next section "Screened datasets". Each perturbation within a batch exists in multiple wells across a variable number of replicate plates. Each well consists of multiple sites, and per-site profiles are derived by averaging features across all single cells available in that site. The MITO-SLOPE metric is then derived from per-site profiles of the RadialDistribution pattern.

To mitigate the effect of plate-to-plate variation in our statistical analysis, we perform a two-sample t-test on per-site MITO-SLOPE values for control versus each perturbation within each plate. We also compare the orthogonal to the target set of features for control versus each perturbation using Hotelling's T^2 test. After forming a set of per-plate t-statistics for each perturbation, we select the plate with the median value of the target metric and retain its statistics as the final phenotype strength properties for that perturbation.

We also derive Cohen's d value and standardized p-value to account for variable sample sizes when comparing each perturbation versus control samples. The final list of perturbations is ranked by Cohen's d values and filtered to include only significant differences according to the corrected p-value using Benjamini-Hochberg multiple hypothesis correction.

Screened datasets

The chemical and genetic perturbation datasets used for virtual screening have previously been published and described. The cpg number allows freely accessing the images and related data from the Cell Painting Gallery (https://github.com/broadinstitute/cellpainting-gallery). Briefly, the datasets include:

- cpg0004-lincs (LINCS, sometimes called LINCS-Pilot1), which is 1,571 compounds across 6 doses in 5 replicates in A549 cells (Way et al. 2022). Images can be viewed here https://idr.github.io/idr0125-way-cellpainting/
- cpg0012-wawer-bioactivecompoundprofiling (CDRP, also called CDRP-BBBC047-Bray), which is 30,430 compounds in U2OS cells at a single dose each, and in 4 replicates per compound (Bray et al. 2017; Wawer et al. 2014). Images can be browsed at Image Data Resource as idr0016.
- cpg0016-jump (JUMP) which is 116,000+ compounds and 15,000+ genes (CRISPR knockout and overexpression) profiled in U2OS cells (Chandrasekaran et al. 2023; Chandrasekaran et al. 2024). Subsets of images can be browsed at third party websites mentioned therein.
- cpg0017-rohban-pathways (TA-ORF, sometimes called TA-ORF-BBBC037-Rohban) which is 323 overexpressed genes in 5 replicates in U2OS cells (Rohban et al. 2017). Images can be browsed at Image Data Resource as idr0033.

Enrichment analysis

We performed an enrichment analysis in Figure 5. Virtual screen analysis of each of the genetic or chemical datasets determines the strength of the target phenotype for each perturbation with respect to the control population through t-test statistics. We sort this differential morphological signature list by the Cohen's d values and inspect enrichment of any candidate gene/compound set towards the top or bottom of the overall set using the GSEA strategy (Subramanian et al. 2005). The degree of a candidate set being overrepresented towards the extremes of the list is evaluated by an enrichment score (ES) which represents the deviation from a uniform distribution of the candidate set throughout the list. To check for statistical significance of a calculated enrichment score, p-values are calculated by forming a null ES distribution and permutation testing. We used blitzGSEA (Lachmann et al. 2022) for the enrichment analysis in Figure 5. Enrichment scores normalized by the size of the gene set (NES) and false discovery rate (FDR) for the presented NES values are reported for each set under enrichment analysis. FDR values are calculated using the Benjamini-Hochberg procedure to correct for multiple hypothesis testing across all gene/compound sets being analyzed.

Data and Code Availability

Raw fibroblast cell images and single cell morphological profiles extracted by CellProfiler are available at http://doi.org/10.5281/zenodo.15390513. The CellProfiler pipelines for extracting them and source code to reproduce and build upon the presented results are available at the project's github repository (https://github.com/carpenter-singh-lab/2025_Haghighi_Mito). Several results files are located in the results subfolder there. We license the source code as BSD 3-Clause, and license the data, results, and figures as CC0 1.0.

Funding

Funding for this study was provided by the National Institutes of Health (NIH MIRA R35 GM122547 to AEC), Merkin Institute Fellowship from the Broad Institute of MIT and Harvard (to AEC), BroadIgnite (to AEC), a NARSAD Distinguished Investigator Award (to BMC), a Harvard-MIT Neurodiscovery program (to BMC), and funds from the Program for Neuropsychiatric Research at McLean Hospital (to BMC). JFH is supported by the Knut and Alice Wallenberg Foundation Postdoc Fellowship program.

Acknowledgements

We gratefully acknowledge input from other members of the Cohen, Cimini and Carpenter–Singh labs as this project developed. In particular, we thank Dr. Yu Han for running preliminary analyses and Dr. Rakesh Karmacharya for manually annotating drugs into mechanism-of-action categories.

Conflicts of interest

The authors disclose no relevant financial relationships to the work presented in this paper.

References

Adlard, P.A. et al., 2008. Rapid restoration of cognition in Alzheimer's transgenic mice with 8-hydroxy quinoline analogs is associated with decreased interstitial Abeta. *Neuron*, 59(1), pp.43–55.

Al-Mehdi, A.-B. et al., 2012. Perinuclear mitochondrial clustering creates an oxidant-rich nuclear domain required for hypoxia-induced transcription. *Science signaling*, 5(231), p.ra47.

Andreassen, O.A. et al., 2013. Improved detection of common variants associated with schizophrenia by leveraging pleiotropy with cardiovascular-disease risk factors. *The American Journal of Human Genetics*, 92(2), pp.197–209.

Anon, CDK18 cyclin dependent kinase 18 [Homo sapiens (human)] - Gene - NCBI. Available at: https://www.ncbi.nlm.nih.gov/gene/5129 [Accessed February 6, 2026a].

Anon, 2021. Recursion and Bayer Expand Fibrosis Collaboration to Include Inferential Search Capabilities. *Recursion website*. Available at: https://ir.recursion.com/news-releases/news-release-details/recursion-and-bayer-expand-fibrosis-collaboration-include [Accessed March 3, 2025].

Anon, SHC1 SHC adaptor protein 1 [Homo sapiens (human)] - Gene - NCBI. Available at: https://www.ncbi.nlm.nih.gov/gene/6464 [Accessed February 6, 2026b].

Antony, P.M.A. et al., 2020. Fibroblast mitochondria in idiopathic Parkinson's disease display morphological changes and enhanced resistance to depolarization. *Scientific reports*, 10(1), p.1569.

Atkin, T.A. et al., 2011. Disrupted in Schizophrenia-1 regulates intracellular trafficking of mitochondria in neurons. *Molecular psychiatry*, 16(2), pp.122–4, 121.

Atkin, T.A., Brandon, N.J. & Kittler, J.T., 2012. Disrupted in Schizophrenia 1 forms pathological aggresomes that disrupt its function in intracellular transport. *Human molecular genetics*, 21(9), pp.2017–2028.

Bareggi, S.R. & Cornelli, U., 2012. Clioquinol: review of its mechanisms of action and clinical uses in neurodegenerative disorders: Clioquinol. *CNS neuroscience & therapeutics*, 18(1), pp.41–46.

Benítez-King, G. et al., 2016. The microtubular cytoskeleton of olfactory neurons derived from patients with schizophrenia or with bipolar disorder: Implications for biomarker characterization, neuronal physiology and pharmacological screening. *Molecular and Cellular Neurosciences*, 73, pp.84–95.

Bessonova, L. et al., 2020. The Economic Burden of Bipolar Disorder in the United States: A Systematic Literature Review. *ClinicoEconomics and outcomes research: CEOR*, 12,

pp.481–497.

Blanchet, L. et al., 2015. Quantifying small molecule phenotypic effects using mitochondrial morpho-functional fingerprinting and machine learning. *Scientific reports*, 5, p.8035.

Bodnar, A.L. et al., 2005. Discovery and structure-activity relationship of quinuclidine benzamides as agonists of alpha7 nicotinic acetylcholine receptors. *Journal of medicinal chemistry*, 48(4), pp.905–908.

Bond, D.J., Lam, R.W. & Yatham, L.N., 2010. Divalproex sodium versus placebo in the treatment of acute bipolar depression: a systematic review and meta-analysis. *Journal of affective disorders*, 124(3), pp.228–234.

Bordbar, A., 2022. Treating cognitive disorders using trapidil. *US Patent*. Available at: https://patentimages.storage.googleapis.com/02/b6/87/eadc02efde59bb/US20220378794A1.pdf [Accessed October 7, 2025].

Bray, M.-A. et al., 2017. A dataset of images and morphological profiles of 30 000 small-molecule treatments using the Cell Painting assay. *GigaScience*, 6(12), pp.1–5.

Brennand, K. et al., 2015. Phenotypic differences in hiPSC NPCs derived from patients with schizophrenia. *Molecular Psychiatry*, 20(3), pp.361–368.

Brodier, L. et al., 2020. A transient decrease in mitochondrial activity is required to establish the ganglion cell fate in retina adapted for high acuity vision. *bioRxiv*. Available at: http://dx.doi.org/10.1101/2020.03.23.002998.

Brown, A.S. et al., 2014. Increased stability of microtubules in cultured olfactory neuroepithelial cells from individuals with schizophrenia. *Progress in Neuro-Psychopharmacology and Biological Psychiatry*, 48, pp.252–258.

Bulik-Sullivan, B. et al., 2015. An atlas of genetic correlations across human diseases and traits. *Nature genetics*, 47(11), pp.1236–1241.

Bulthuis, E.P. et al., 2019. Mitochondrial Morphofunction in Mammalian Cells. *Antioxidants & redox signaling*, 30(18), pp.2066–2109.

Carling, P.J. et al., 2020. Deep phenotyping of peripheral tissue facilitates mechanistic disease stratification in sporadic Parkinson's disease. *Progress in Neurobiology*, 187(101772), p.101772.

Carlson, G.A. & Goodwin, F.K., 1973. The stages of mania. A longitudinal analysis of the manic episode. *Archives of general psychiatry*, 28(2), pp.221–228.

Cataldo, A.M. et al., 2010. Abnormalities in mitochondrial structure in cells from patients with bipolar disorder. *The American journal of pathology*, 177(2), pp.575–585.

Celik, S. et al., 2024. Building, benchmarking, and exploring perturbative maps of

transcriptional and morphological data. *PLoS computational biology*, 20(10), p.e1012463.

Chan, D.C., 2020. Mitochondrial Dynamics and Its Involvement in Disease. *Annual review of pathology*, 15, pp.235–259.

Chandrasekaran, S.N. et al., 2020. Image-based profiling for drug discovery: due for a machine-learning upgrade? *Nature reviews. Drug discovery*, pp.1–15.

Chandrasekaran, S.N. et al., 2023. JUMP Cell Painting dataset: morphological impact of 136,000 chemical and genetic perturbations. *bioRxiv*, p.2023.03.23.534023. Available at: https://www.biorxiv.org/content/biorxiv/early/2023/03/24/2023.03.23.534023 [Accessed May 1, 2023].

Chandrasekaran, S.N. et al., 2024. Morphological map of under- and over-expression of genes in human cells. *bioRxiv*. Available at: https://www.biorxiv.org/content/10.1101/2024.12.02.624527.

Chen, H. et al., 2024. Mitochondrial dynamics dysfunction: Unraveling the hidden link to depression. *Biomedecine & pharmacotherapie [Biomedicine & pharmacotherapy]*, 175(116656), p.116656.

Chen, Y. et al., 2024. PI3K-AKT/mTOR signaling in psychiatric disorders: A valuable target to stimulate or suppress? *The international journal of neuropsychopharmacology*, 27(2). Available at: https://pubmed.ncbi.nlm.nih.gov/38365306/.

Chu, C.-H. et al., 2022. Image analysis of the mitochondrial network morphology with applications in cancer research. *Frontiers in Physics*, 10(855775). Available at: http://dx.doi.org/10.3389/fphy.2022.855775.

Cipriani, A. et al., 2013. Valproic acid, valproate and divalproex in the maintenance treatment of bipolar disorder. *Cochrane database of systematic reviews*, (10), p.CD003196.

Citron, B.A. et al., 2008. Transcription factor Sp1 dysregulation in Alzheimer's disease. *Journal of neuroscience research*, 86(11), pp.2499–2504.

Cohen, B.M. & Öngür, D., 2018. The urgent need for more research on bipolar depression. *The lancet. Psychiatry*, 5(12), pp.e29–e30.

Corena-McLeod, M. et al., 2013. New model of action for mood stabilizers: phosphoproteome from rat pre-frontal cortex synaptoneurosomal preparations. *PloS one*, 8(5), p.e52147.

Cuccarese, M.F. et al., 2020. Functional immune mapping with deep-learning enabled phenomics applied to immunomodulatory and COVID-19 drug discovery. *bioRxiv*, p.2020.08.02.233064. Available at:

https://www.biorxiv.org/content/10.1101/2020.08.02.233064v2 [Accessed January 27, 2023].

Culmsee, C. et al., 2018. Mitochondria, Microglia, and the Immune System-How Are They Linked in Affective Disorders? *Frontiers in psychiatry / Frontiers Research Foundation*, 9, p.739.

Cuperfain, A.B. et al., 2018. The Complex Interaction of Mitochondrial Genetics and Mitochondrial Pathways in Psychiatric Disease. *Molecular neuropsychiatry*, 4(1), pp.52–69.

Delhaye, S. & Bardoni, B., 2021. Role of phosphodiesterases in the pathophysiology of neurodevelopmental disorders. *Molecular psychiatry*, 26(9), pp.4570–4582.

DeMartinis, N., 3rd et al., 2019. A proof-of-concept study evaluating the phosphodiesterase 10A inhibitor PF-02545920 in the adjunctive treatment of suboptimally controlled symptoms of schizophrenia. *Journal of clinical psychopharmacology*, 39(4), pp.318–328.

Dhar, S.S., Johar, K. & Wong-Riley, M.T.T., 2013. Bigenomic transcriptional regulation of all thirteen cytochrome c oxidase subunit genes by specificity protein 1. *Open biology*, 3(3), p.120176.

Ding, J.B. & Hu, K., 2021. Cigarette smoking and schizophrenia: Etiology, clinical, pharmacological, and treatment implications. *Schizophrenia research and treatment*, 2021(1), p.7698030.

Dragich, J.M. et al., 2016. Autophagy linked FYVE (Alfy/WDFY3) is required for establishing neuronal connectivity in the mammalian brain. *eLife*, 5, p.e14810.

Drewes, G. et al., 1997. MARK, a novel family of protein kinases that phosphorylate microtubule-associated proteins and trigger microtubule disruption. *Cell*, 89(2), pp.297–308.

Erhardt, S. et al., 2017. The kynurenine pathway in schizophrenia and bipolar disorder. *Neuropharmacology*, 112(Pt B), pp.297–306.

Fay, M.M. et al., 2023. RxRx3: Phenomics Map of Biology. *Systems Biology*. Available at: https://www.biorxiv.org/content/10.1101/2023.02.07.527350v1.

Ferguson, M.W. et al., 2022. Current and possible future therapeutic options for Huntington's disease. *Journal of central nervous system disease*, 14, p.11795735221092517.

Fessler, E. et al., 2020. A pathway coordinated by DELE1 relays mitochondrial stress to the cytosol. *Nature*, 579(7799), pp.433–437.

Finley, K.D. et al., 2003. Blue cheese mutations define a novel, conserved gene involved in progressive neural degeneration. *The Journal of neuroscience: the official journal of the Society for Neuroscience*, 23(4), pp.1254–1264.

Fischer, N.C. et al., 2022. The ANC-1 (Nesprin-1/2) organelle-anchoring protein functions through mitochondria to polarize axon growth in response to SLT-1. *PLoS genetics*, 18(11), p.e1010521.

Flippo, K.H. & Strack, S., 2017. An emerging role for mitochondrial dynamics in schizophrenia. *Schizophrenia research*, 187, pp.26–32.

Franceschi, S. et al., 2022. Sedoheptulose kinase SHPK expression in glioblastoma: Emerging role of the nonoxidative pentose phosphate pathway in tumor proliferation. *International journal of molecular sciences*, 23(11), p.5978.

GeneCards Human Gene Database, DCTN4 Gene - GeneCards. Available at: https://www.genecards.org/cgi-bin/carddisp.pl?gene=DCTN4 [Accessed September 12, 2025].

Giménez-Palomo, A. et al., 2021. The Role of Mitochondria in Mood Disorders: From Physiology to Pathophysiology and to Treatment. *Frontiers in psychiatry / Frontiers Research Foundation*, 12, p.546801.

Goering, R. et al., 2023. RNA localization mechanisms transcend cell morphology. *eLife*, 12, p.e80040.

Gray, J.A. & Roth, B.L., 2007. The pipeline and future of drug development in schizophrenia. *Molecular psychiatry*, 12(10), pp.904–922.

Grotzinger, A.D. et al., 2023. Transcriptome-Wide Structural Equation Modeling of 13 Major Psychiatric Disorders for Cross-Disorder Risk and Drug Repurposing. *JAMA psychiatry* . Available at: http://dx.doi.org/10.1001/jamapsychiatry.2023.1808.

Haitina, T. et al., 2006. Fourteen novel human members of mitochondrial solute carrier family 25 (SLC25) widely expressed in the central nervous system. *Genomics*, 88(6), pp.779–790.

Han, X.-C. et al., 2025. KCNH6 potassium channel regulates assembling of mitochondrial complex I and promotes insulin secretion in islet beta cells. *FASEB journal: official publication of the Federation of American Societies for Experimental Biology*, 39(12), p.e70776.

Harrison, P.J., Colbourne, L. & Harrison, C.H., 2020. The neuropathology of bipolar disorder: systematic review and meta-analysis. *Molecular psychiatry*, 25(8), pp.1787–1808.

Harris, S.E. et al., 2020. Neurology-related protein biomarkers are associated with cognitive ability and brain volume in older age. *Nature communications*, 11(1), p.800.

Harwig, M.C. et al., 2018. Methods for imaging mammalian mitochondrial morphology: A prospective on MitoGraph. *Analytical Biochemistry*, 552, pp.81–99.

Hebb, A.L.O. & Robertson, H.A., 2007. Role of phosphodiesterases in neurological and psychiatric disease. *Current opinion in pharmacology*, 7(1), pp.86–92.

Heffner, J.L. et al., 2011. The co-occurrence of cigarette smoking and bipolar disorder: phenomenology and treatment considerations: Cigarette smoking and bipolar disorder. *Bipolar disorders*, 13(5-6), pp.439–453.

Helguera, P. et al., 2005. ets-2 promotes the activation of a mitochondrial death pathway in Down's syndrome neurons. *The Journal of Neuroscience: The Official Journal of the Society for Neuroscience*, 25(9), pp.2295–2303.

Hemel, I.M.G.M. et al., 2021. A hitchhiker's guide to mitochondrial quantification. *Mitochondrion*, 59, pp.216–224.

Hirabayashi, Y. et al., 2024. Most axonal mitochondria in cortical pyramidal neurons lack mitochondrial DNA and consume ATP. *bioRxiv*. Available at: https://www.biorxiv.org/content/10.1101/2024.02.12.579972v1.full.

Hung, C.L.-K. et al., 2018. A patient-derived cellular model for Huntington's disease reveals phenotypes at clinically relevant CAG lengths. *Molecular biology of the cell*, 29(23), pp.2809–2820.

Jash, S. et al., 2019. CIDEA transcriptionally regulates UCP1 for britening and thermogenesis in human fat cells. *iScience*, 20, pp.73–89.

Jenkins, B.C. et al., 2024. Mitochondria in disease: changes in shapes and dynamics. *Trends in biochemical sciences*, 49(4), pp.346–360.

Jiang, M. et al., 2023. Phosphodiesterase and psychiatric disorders: a two-sample Mendelian randomization study. *Journal of translational medicine*, 21(1), p.560.

Jope, R.S. & Roh, M.-S., 2006. Glycogen synthase kinase-3 (GSK3) in psychiatric diseases and therapeutic interventions. *Current drug targets*, 7(11), pp.1421–1434.

Kadakia, A. et al., 2022. The economic burden of schizophrenia in the United States. *The Journal of clinical psychiatry*, 83(6). Available at: https://www.psychiatrist.com/jcp/schizophrenia/economic-burden-schizophrenia-united-states/.

Kessi, M. et al., 2023. Disruption of mitochondrial and lysosomal functions by human CACNA1C variants expressed in HEK 293 and CHO cells. *Frontiers in molecular neuroscience*, 16, p.1209760.

Kuperberg, M., Greenebaum, S.L.A. & Nierenberg, A.A., 2021. Targeting Mitochondrial

Dysfunction for Bipolar Disorder. In A. H. Young & M. F. Juruena, eds. *Bipolar Disorder: From Neuroscience to Treatment*. Cham: Springer International Publishing, pp. 61–99.

Kwon, S.-K. et al., 2016. LKB1 regulates mitochondria-dependent presynaptic calcium clearance and neurotransmitter release properties at excitatory synapses along cortical axons. *PLoS biology*, 14(7), p.e1002516.

Lachmann, A., Xie, Z. & Ma'ayan, A., 2022. blitzGSEA: efficient computation of gene set enrichment analysis through gamma distribution approximation. *Bioinformatics* , 38(8), pp.2356–2357.

Langhammer, F. et al., 2023. Genotype-phenotype correlations in RHOBTB2-associated neurodevelopmental disorders. *Genetics in medicine: official journal of the American College of Medical Genetics*, 25(8), p.100885.

Leonard, A.P. et al., 2015. Quantitative analysis of mitochondrial morphology and membrane potential in living cells using high-content imaging, machine learning, and morphological binning. *Biochimica et biophysica acta*, 1853(2), pp.348–360.

Lim, A. & Kraut, R., 2009. The Drosophila BEACH family protein, blue cheese, links lysosomal axon transport with motor neuron degeneration. *The Journal of neuroscience: the official journal of the Society for Neuroscience*, 29(4), pp.951–963.

Lin, C., Zhang, X. & Jin, H., 2022. The Societal Cost of Schizophrenia: An Updated Systematic Review of Cost-of-Illness Studies. *PharmacoEconomics*. Available at: http://dx.doi.org/10.1007/s40273-022-01217-8.

Lones, M.A., 2021. How to avoid machine learning pitfalls: a guide for academic researchers. *arXiv [cs.LG]*. Available at: http://arxiv.org/abs/2108.02497.

Mandal, A. & Drerup, C.M., 2019. Axonal Transport and Mitochondrial Function in Neurons. *Frontiers in cellular neuroscience*, 13, p.373.

Marchisella, F., Coffey, E.T. & Hollos, P., 2016. Microtubule and microtubule associated protein anomalies in psychiatric disease. *Cytoskeleton (Hoboken, N.J.)*, 73(10), pp.596–611.

Marques, A.P. et al., 2021. Mitochondrial Alterations in Fibroblasts of Early Stage Bipolar Disorder Patients. *Biomedicines*, 9(5). Available at: http://dx.doi.org/10.3390/biomedicines9050522.

Marshall, R.D., Menniti, F.S. & Tepper, M.A., 2024. A novel PDE10A inhibitor for Tourette syndrome and other movement disorders. *Cells (Basel, Switzerland)*, 13(14), p.1230.

Martin, R. et al., 2019. De novo variants in CNOT3 cause a variable neurodevelopmental disorder. *European journal of human genetics: EJHG*, 27(11), pp.1677–1682.

McDiarmid, A.H. et al., 2023. Morphological profiling by Cell Painting in human neural progenitor cells classifies hit compounds in a pilot drug screen for Alzheimer's disease. *bioRxiv*, p.2023.01.16.523559. Available at: https://www.biorxiv.org/content/10.1101/2023.01.16.523559v1 [Accessed January 21, 2023].

McIntyre, R.S. et al., 2020. Bipolar disorders. *The Lancet*, 396(10265), pp.1841–1856.

McKeny, P.T., Nessel, T.A. & Zito, P.M., 2025. Antifungal antibiotics. In *StatPearls*. Treasure Island (FL): StatPearls Publishing.

McPhie, D.L. et al., 2018. Oligodendrocyte differentiation of induced pluripotent stem cells derived from subjects with schizophrenias implicate abnormalities in development. *Translational psychiatry*, 8(1), p.230.

McPhie, M.L., Bridgman, A.C. & Kirchhof, M.G., 2021. A Review of Skin Disease in Schizophrenia. *Dermatology* , 237(2), pp.248–261.

McQuin, C. et al., 2018. CellProfiler 3.0: Next-generation image processing for biology. *PLoS biology*, 16(7), p.e2005970.

Mertens, J. et al., 2015. Differential responses to lithium in hyperexcitable neurons from patients with bipolar disorder. *Nature*, 527(7576), pp.95–99.

Michels, S. et al., 2018. Downregulation of the psychiatric susceptibility gene Cacna1c promotes mitochondrial resilience to oxidative stress in neuronal cells. *Cell death discovery*, 4, p.54.

Miyamoto, S. et al., 2025. Mutant-specific dysfunction of RHOBTB2 impairs mitochondrial function and Na+/K+-ATPase levels in a cell model. *Biochimica et biophysica acta. Molecular cell research*, 1873(3), p.120103.

Moon, A.L. et al., 2018. CACNA1C: Association with psychiatric disorders, behavior, and neurogenesis. *Schizophrenia bulletin*, 44(5), pp.958–965.

Mortiboys, H. et al., 2008. Mitochondrial function and morphology are impaired in parkin-mutant fibroblasts. *Annals of Neurology*, 64(5), pp.555–565.

Mortiboys, H. et al., 2010. Mitochondrial impairment in patients with Parkinson disease with the G2019S mutation in LRRK2. *Neurology*, 75(22), pp.2017–2020.

Munakata, K. et al., 2004. Mitochondrial DNA 3644T-->C mutation associated with bipolar disorder. *Genomics*, 84(6), pp.1041–1050.

Murphy, L.C. & Millar, J.K., 2017. Regulation of mitochondrial dynamics by DISC1, a putative risk factor for major mental illness. *Schizophrenia research*, 187, pp.55–61.

Napoli, E. et al., 2021. Wdfy3 regulates glycophagy, mitophagy, and synaptic plasticity.

Journal of Cerebral Blood Flow and Metabolism: Official Journal of the International Society of Cerebral Blood Flow and Metabolism, 41(12), pp.3213–3231.

Neumann, C. et al., 2024. Abstract 7133: Phenomics-enabled discovery and optimization of small-molecule RBM39 degraders as an alternative to CDK12 targeting in high-grade serous ovarian cancer (HGSOC). *Cancer Research*, 84(6_Supplement), pp.7133–7133.

Niculescu, A.B. et al., 2019. Towards precision medicine for pain: diagnostic biomarkers and repurposed drugs. *Molecular psychiatry*, 24(4), pp.501–522.

Ni, P., Ma, Y. & Chung, S., 2024. Mitochondrial dysfunction in psychiatric disorders. *Schizophrenia research*, 273, pp.62–77.

Olesen, M.A., Villavicencio-Tejo, F. & Quintanilla, R.A., 2022. The use of fibroblasts as a valuable strategy for studying mitochondrial impairment in neurological disorders. *Translational Neurodegeneration*, 11(1), p.36.

Panchision, D.M., 2016. Concise Review: Progress and Challenges in Using Human Stem Cells for Biological and Therapeutics Discovery: Neuropsychiatric Disorders. *Stem cells*, 34(3), pp.523–536.

Papageorgiou, M.P. & Filiou, M.D., 2024. Mitochondrial dynamics and psychiatric disorders: The missing link. *Neuroscience and biobehavioral reviews*, 165(105837), p.105837.

Payne, T. et al., 2024. Multimodal assessment of mitochondrial function in Parkinson's disease. *Brain: A Journal of Neurology*, 147(1), pp.267–280.

Pereira, C. et al., 2018. Mitochondrial Agents for Bipolar Disorder. *The international journal of neuropsychopharmacology / official scientific journal of the Collegium Internationale Neuropsychopharmacologicum* , 21(6), pp.550–569.

Perrottelli, A. et al., Advances in the understanding of the pathophysiology of schizophrenia and bipolar disorder through induced pluripotent stem cell models. Available at: http://dx.doi.org/10.1503/jpn.230112.

Pilling, A.D. et al., 2006. Kinesin-1 and Dynein are the primary motors for fast transport of mitochondria in Drosophila motor axons. *Molecular biology of the cell*, 17(4), pp.2057–2068.

Pinacho, R. et al., 2014. Increased SP4 and SP1 transcription factor expression in the postmortem hippocampus of chronic schizophrenia. *Journal of psychiatric research*, 58, pp.189–196.

Plitman, E. et al., 2017. Kynurenic acid in schizophrenia: A systematic review and meta-analysis. *Schizophrenia bulletin*, 43(4), pp.764–777.

Qian, X., Song, H. & Ming, G.-L., 2019. Brain organoids: advances, applications and

challenges. *Development* , 146(8). Available at: http://dx.doi.org/10.1242/dev.166074.

Qi, H.A.O. et al., Nuclear staining with MitoTracker® Orange CMTMRos (Thermo Fisher Scientific, cat. no. M7510)? *ResearchGate*. Available at: https://www.researchgate.net/post/Nuclear-staining-with-MitoTrackerR-Orange-CMTMRos-Thermo-Fisher-Scientific-cat-no-M7510 [Accessed February 10, 2026].

Rahman, M., Awosika, A.O. & Nguyen, H., 2025. Valproic acid. In *StatPearls*. Treasure Island (FL): StatPearls Publishing.

Rampino, A. et al., 2021. Involvement of vascular endothelial growth factor in schizophrenia. *Neuroscience letters*, 760(136093), p.136093.

Ripoll, N., Bronnec, M. & Bourin, M., 2004. Nicotinic receptors and schizophrenia. *Current medical research and opinion*, 20(7), pp.1057–1074.

Rivelli, A. et al., 2022. Prevalence of mental health conditions among 6078 individuals with Down syndrome in the United States. *Journal of patient-centered research and reviews*, 9(1), pp.58–63.

Roberts, R.C., 2021. Mitochondrial dysfunction in schizophrenia: With a focus on postmortem studies. *Mitochondrion*, 56, pp.91–101.

Robicsek, O. et al., 2013. Abnormal neuronal differentiation and mitochondrial dysfunction in hair follicle-derived induced pluripotent stem cells of schizophrenia patients. *Molecular Psychiatry*, 18(10), pp.1067–1076.

Rohban, M.H. et al., 2017. Systematic morphological profiling of human gene and allele function via Cell Painting. *eLife*, 6. Available at: http://dx.doi.org/10.7554/eLife.24060.

Rohban, M.H. et al., 2022. Virtual screening for small-molecule pathway regulators by image-profile matching. *Cell systems*, 13(9), pp.724–736.e9.

Rosenfeld, M. et al., 2011. Perturbation in mitochondrial network dynamics and in complex I dependent cellular respiration in schizophrenia. *Biological psychiatry*, 69(10), pp.980–988.

Sadeghi, M.A. et al., 2023. Phosphodiesterase inhibitors in psychiatric disorders. *Psychopharmacology*, 240(6), pp.1201–1219.

Santpere, G. et al., 2006. Abnormal Sp1 transcription factor expression in Alzheimer disease and tauopathies. *Neuroscience letters*, 397(1-2), pp.30–34.

Sato, Y. et al., 1998. Three-dimensional multi-scale line filter for segmentation and visualization of curvilinear structures in medical images. *Medical Image Analysis*, 2(2), pp.143–168.

Saxton, W.M. & Hollenbeck, P.J., 2012. The axonal transport of mitochondria. *Journal of cell science*, 125(Pt 9), pp.2095–2104.

Scaini, G. et al., 2021. Mitochondrial dysfunction as a critical event in the pathophysiology of bipolar disorder. *Mitochondrion*, 57, pp.23–36.

Scaini, G. et al., 2016. Mitochondrial dysfunction in bipolar disorder: Evidence, pathophysiology and translational implications. *Neuroscience and biobehavioral reviews*, 68, pp.694–713.

Scaini, G. et al., 2017. Perturbations in the apoptotic pathway and mitochondrial network dynamics in peripheral blood mononuclear cells from bipolar disorder patients. *Translational psychiatry*, 7(5), p.e1111.

Schiff, L. et al., 2022. Integrating deep learning and unbiased automated high-content screening to identify complex disease signatures in human fibroblasts. *Nature communications*, 13(1), p.1590.

Sharbaf Shoar, N., Fariba, K.A. & Padhy, R.K., 2025. Citalopram. In *StatPearls*. Treasure Island (FL): StatPearls Publishing.

Shi, X. et al., 2022. Hierarchical deployment of Tbx3 dictates the identity of hypothalamic KNDy neurons to control puberty onset. *Science advances*, 8(46), p.eabq2987.

Sklar, P. et al., 2008. Whole-genome association study of bipolar disorder. *Molecular psychiatry*, 13(6), pp.558–569.

Smith, G.A. et al., 2016. Fibroblast biomarkers of sporadic Parkinson's disease and LRRK2 kinase inhibition. *Molecular Neurobiology*, 53(8), pp.5161–5177.

Smith, J., Mowla, S. & Prince, S., 2011. Basal transcription of the human TBX3 gene, a key developmental regulator which is overexpressed in several cancers, requires functional NF-Y and Sp1 sites. *Gene*, 486(1-2), pp.41–46.

Snelleksz, M. & Dean, B., 2021. Lower levels of tubulin alpha 1b in the frontal pole in schizophrenia supports a role for changed cytoskeletal dynamics in the aetiology of the disorder. *Psychiatry Research*, 303(114096), p.114096.

Snitow, M.E., Bhansali, R.S. & Klein, P.S., 2021. Lithium and therapeutic targeting of GSK-3. *Cells (Basel, Switzerland)*, 10(2), p.255.

Stankey, C.T. et al., 2024. A disease-associated gene desert directs macrophage inflammation through ETS2. *Nature*, 630(8016), pp.447–456.

Stępnicki, P., Kondej, M. & Kaczor, A.A., 2018. Current Concepts and Treatments of Schizophrenia. *Molecules* , 23(8). Available at: http://dx.doi.org/10.3390/molecules23082087.

Stirling, D.R. et al., 2021. CellProfiler 4: improvements in speed, utility and usability. *BMC bioinformatics*, 22(1), p.433.

Subramanian, A. et al., 2005. Gene set enrichment analysis: a knowledge-based approach for interpreting genome-wide expression profiles. *Proceedings of the National Academy of Sciences of the United States of America*, 102(43), pp.15545–15550.

Suh, B.K. et al., 2021. Schizophrenia-associated dysbindin modulates axonal mitochondrial movement in cooperation with p150glued. *Molecular brain*, 14(1), p.14.

Sutton, L.P. & Rushlow, W.J., 2011. The effects of neuropsychiatric drugs on glycogen synthase kinase-3 signaling. *Neuroscience*, 199, pp.116–124.

Suzuki, T. et al., 2015. CNOT3 suppression promotes necroptosis by stabilizing mRNAs for cell death-inducing proteins. *Scientific Reports*, 5(1), p.14779.

Tan, H.-Y., Cho, H. & Lee, L.P., 2021. Human mini-brain models. *Nature biomedical engineering*, 5(1), pp.11–25.

Tegtmeyer, M. et al., 2024. Combining NeuroPainting with transcriptomics reveals cell-type-specific morphological and molecular signatures of the 22q11.2 deletion. *bioRxivorg*. Available at: https://www.biorxiv.org/content/10.1101/2024.11.16.623947.

Teves, J.M.Y. et al., 2017. Parkinson's disease skin fibroblasts display signature alterations in growth, redox homeostasis, mitochondrial function, and autophagy. *Frontiers in Neuroscience*, 11, p.737.

Thanseem, I. et al., 2012. Elevated transcription factor specificity protein 1 in autistic brains alters the expression of autism candidate genes. *Biological psychiatry*, 71(5), pp.410–418.

Theeuwes, W.F. et al., 2018. Inactivation of glycogen synthase kinase 3β (GSK-3β) enhances mitochondrial biogenesis during myogenesis. *Biochimica et biophysica acta. Molecular basis of disease*, 1864(9 Pt B), pp.2913–2926.

Thomas, R.A. et al., 2023. A deep learning convolutional neural network distinguishes neuronal models of Parkinson's disease from matched controls. *Neuroscience*. Available at: https://www.biorxiv.org/content/10.1101/2023.11.23.568499v1.full.

Thomsen, M.S., Weyn, A. & Mikkelsen, J.D., 2011. Hippocampal α7 nicotinic acetylcholine receptor levels in patients with schizophrenia, bipolar disorder, or major depressive disorder: α7 nAChR in mental disorders. *Bipolar disorders*, 13(7-8), pp.701–707.

Trubetskoy, V. et al., 2022. Mapping genomic loci implicates genes and synaptic biology in schizophrenia. *Nature*, 604(7906), pp.502–508.

Vaccaro, V. et al., 2017. Miro1-dependent mitochondrial positioning drives the rescaling of presynaptic Ca2+ signals during homeostatic plasticity. *EMBO reports*, 18(2), pp.231–240.

Varidaki, A., Hong, Y. & Coffey, E.T., 2018. Repositioning microtubule stabilizing drugs for brain disorders. *Frontiers in Cellular Neuroscience*, 12, p.226.

Wali, G. et al., 2023. Pharmacological rescue of mitochondrial and neuronal defects in SPG7 hereditary spastic paraplegia patient neurons using high throughput assays. *Frontiers in neuroscience*, 17, p.1231584.

Wali, G. et al., 2021. Single cell morphology distinguishes genotype and drug effect in Hereditary Spastic Paraplegia. *Scientific reports*, 11(1), p.16635.

Walling, D.P. et al., 2019. Phosphodiesterase 10A inhibitor monotherapy is not an effective treatment of acute schizophrenia. *Journal of clinical psychopharmacology*, 39(6), pp.575–582.

Wang, H. et al., 2023. Neurotrophic basis to the pathogenesis of depression and phytotherapy. *Frontiers in pharmacology*, 14, p.1182666.

Wawer, M.J. et al., 2014. Toward performance-diverse small-molecule libraries for cell-based phenotypic screening using multiplexed high-dimensional profiling. *Proceedings of the National Academy of Sciences of the United States of America*, 111(30), pp.10911–10916.

Way, G.P. et al., 2022. Morphology and gene expression profiling provide complementary information for mapping cell state. *Cell systems*, 13(11), pp.911–923.e9.

Whelan, D.R. & Bell, T.D.M., 2015. Image artifacts in single molecule localization microscopy: why optimization of sample preparation protocols matters. *Scientific reports*, 5(1), p.7924.

Willman, C. & Tadi, P., 2025. Tolcapone. In *StatPearls*. Treasure Island (FL): StatPearls Publishing.

Willmore, L.J., 2003. Divalproex and epilepsy. *Psychopharmacology bulletin*, 37 Suppl 2, pp.43–53.

Wu, Y., Chen, M. & Jiang, J., 2019. Mitochondrial dysfunction in neurodegenerative diseases and drug targets via apoptotic signaling. *Mitochondrion*, 49, pp.35–45.

Yang, K. et al., 2017. The key roles of GSK-3β in regulating mitochondrial activity. *Cellular physiology and biochemistry: international journal of experimental cellular physiology, biochemistry, and pharmacology*, 44(4), pp.1445–1459.

Yang, S.J. et al., 2019. Applying Deep Neural Network Analysis to High-Content Image-Based

Assays. *SLAS Discovery*, 24(8), pp.829–841. Available at: http://dx.doi.org/10.1177/2472555219857715.

Yatchenko, Y. & Ben-Shachar, D., 2021. Update of mitochondrial network analysis by imaging: Proof of technique in schizophrenia. *Methods in Molecular Biology (Clifton, N.J.)*, 2277, pp.187–201.

Zanfardino, P. et al., 2021. Tackling Dysfunction of Mitochondrial Bioenergetics in the Brain. *International journal of molecular sciences*, 22(15). Available at: http://dx.doi.org/10.3390/ijms22158325.

Zhang, Y.-C. et al., 2022. KCNH6 enhanced hepatic glucose metabolism through mitochondrial Ca2+ regulation and oxidative stress inhibition. *Oxidative medicine and cellular longevity*, 2022(1), p.3739556.

Zhao, R., Lu, J. & Xiong, F., 2023. 1597-P: KCNH6 regulates hepatic mitochondrial function and glucose metabolism via NF-κB pathway. *Diabetes*, 72(Supplement_1), p.1597–P.

Zheng, Y.-R., Zhang, X.-N. & Chen, Z., 2019. Mitochondrial transport serves as a mitochondrial quality control strategy in axons: Implications for central nervous system disorders. *CNS neuroscience & therapeutics*, 25(7), pp.876–886.

Supplementary information

Haghighi, McPhie, et al.

Supplementary Table 1: Subject demographics, comorbid conditions, and medications at time of biopsy. A summary of diagnosis, sex, and age is provided as Supplementary Figure 1.
<This Word document is provided as a supplemental file with the paper>

Category	Healthy controls	Schizophrenias	Bipolar Disorders	Depression
Number of patients	48	50	50	20
SCID Dx	48 HC	38 SZ/11 SZA/1 Psy NOS	48 BPI/2BPII	20 MDD
SEX	17 F/ 31 M	11 F/ 39 M	14 F/ 36 M	10 F/ 10M
Mean age at skin biopsy	35.8± 12.6 yr	37.0 ± 13.4 yr	35.5 ±13.1 yr	31.3 ± 11.4 yr
Age range at skin biopsy	20-65	18-68	19-69	18-55

Supplementary Figure 1. Characteristics of patients in the study

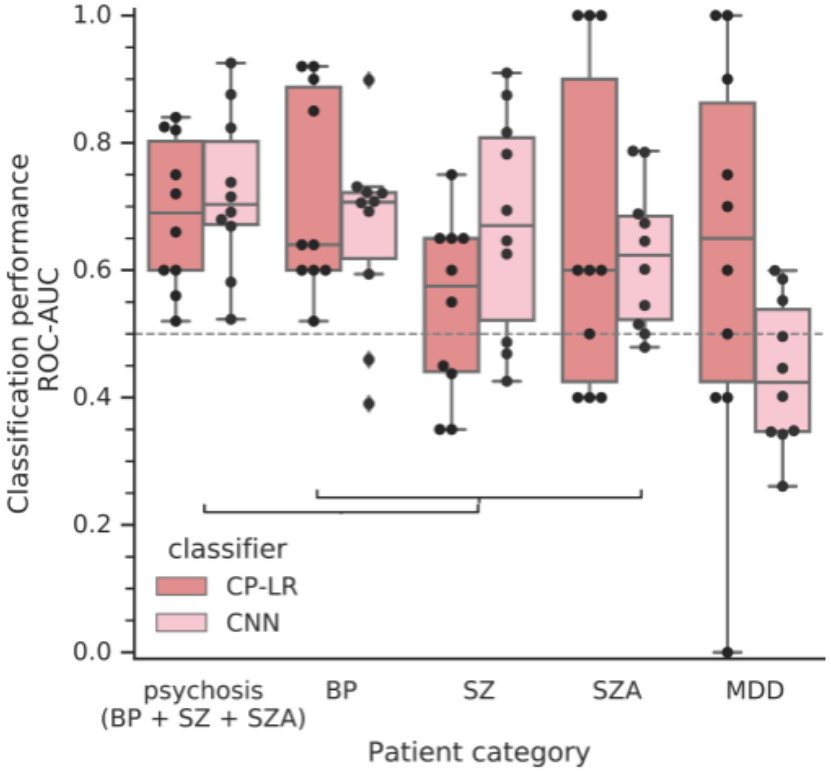

Supplementary Figure 2. Machine learning classification can distinguish several patient groups from healthy controls: comparison of logistic regression applied to the CellProfiler features patient-level profiles versus deep learning end to end single cell classification. A: Classification using a Logistic Regression (LR) model on CellProfiler (CP) features for classification of patients (CP-LR). Patient-level profiles were formed using classical image-based single-cell features extracted using CellProfiler software, limited to mitochondrial features. B: Raw single-cell images of the mitochondrial channel were used for a deep learning classifier, a convolutional neural network (CNN). Patient categories include a primary diagnosis of bipolar disorder (BP), Schizophrenia (SZ), Schizoaffective disorder (SZA), and depression or major depressive disorder (MDD). Psychosis includes patients in classes BP, SZ, and SZA. Classifiers are evaluated by k-fold (k=10) cross validation and the distribution of area under the receiver operating characteristic curve (AUC-ROC) for each binary classification in each validation partition are reported as the data points comprising the box plots, which show 25th and 75th percentile, with the median marked as a line. Features used in the classification include all MitoTracker related features except those measuring correlation to other channels.

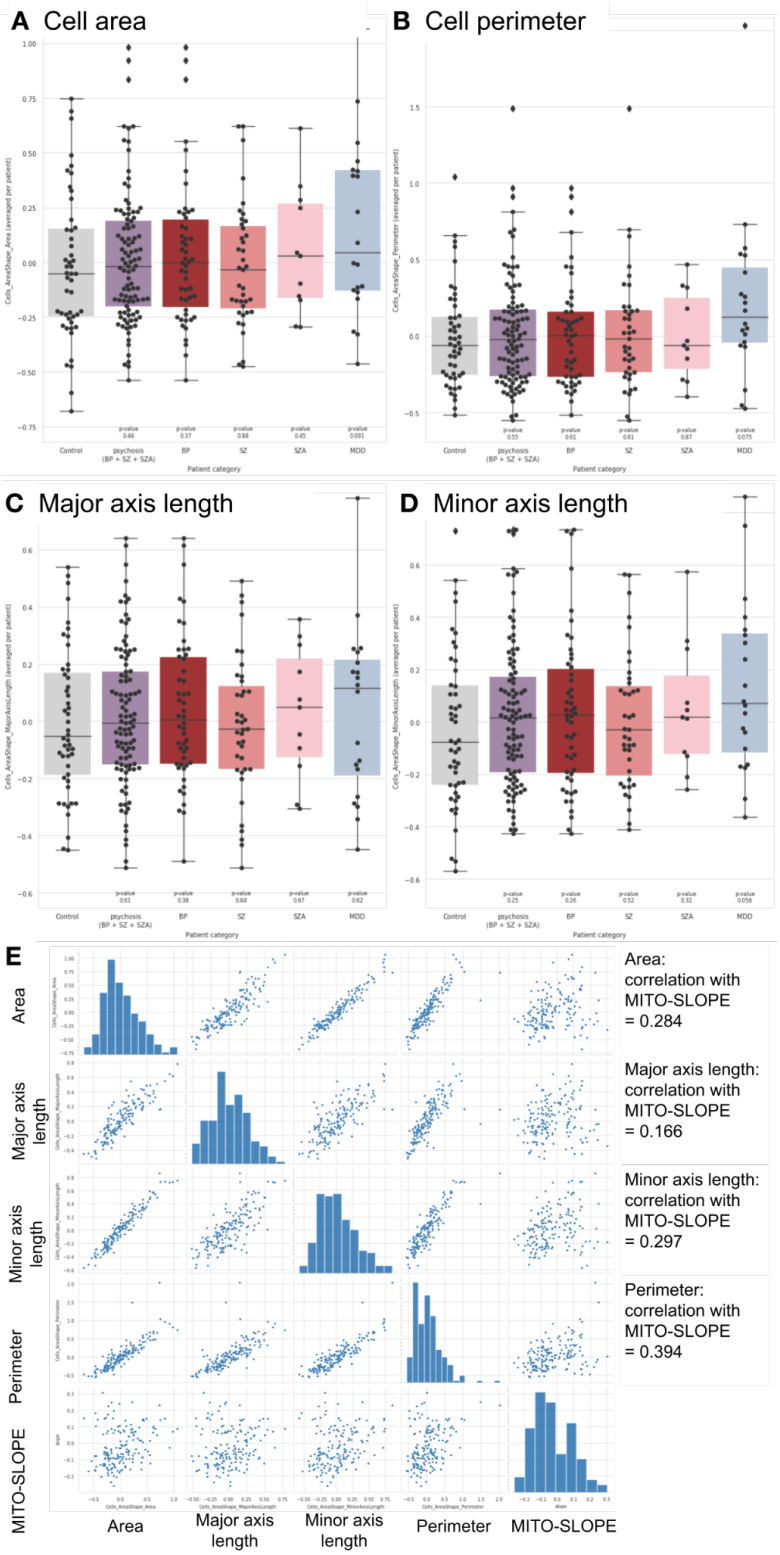

Supplementary Figure 3. Various metrics of cell size do not distinguish various patient categories (A. area, B. perimeter, C. major axis length, D. minor axis length). Data display is the same as in Figure 4C. E. Cell size metrics correlate strongly with each other but correlate less than 0.40 with MITO-SLOPE.

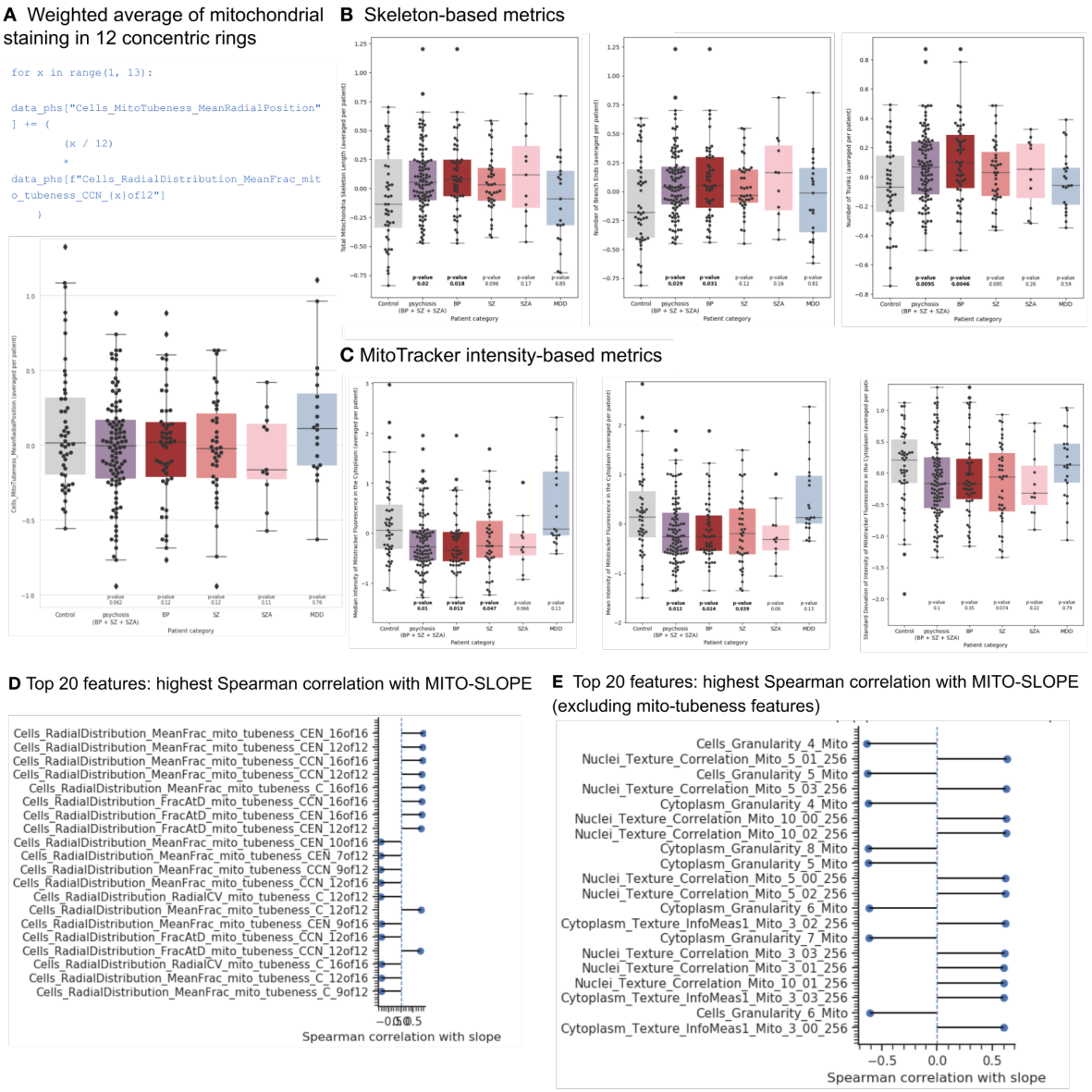

Supplementary Figure 4. Various alternative metrics to characterize mitochondria. Plots for A-C are as in Figure 4C. A) Weighted average of mitochondrial staining in 12 concentric rings following the formula shown. B) Skeleton-based metrics involve thresholding and skeletonizing the mitochondrial network and using CellProfiler's MeasureSkeleton module to measure various properties. This module measures the number of trunks and branches for each branching system in an image. The module takes a skeletonized image of the object plus previously identified seed objects (in this case, nuclei) and finds the number of trunks that emerge from the seed object and the number of branches along the trunks. Metrics shown are TotalObjectSkeletonLength (the length of all skeleton segments per object), NumberBranchEnds (the number of branch end-points, i.e, termini), and NumberTrunks (the number of trunks, i.e., branchpoints that lie within the seed objects). C) MitoTracker intensity-based metrics include the median, mean, and standard deviation of the intensity of MitoTracker staining in the cytoplasm. D & E) Listing of features highly correlated with MITO-SLOPE.

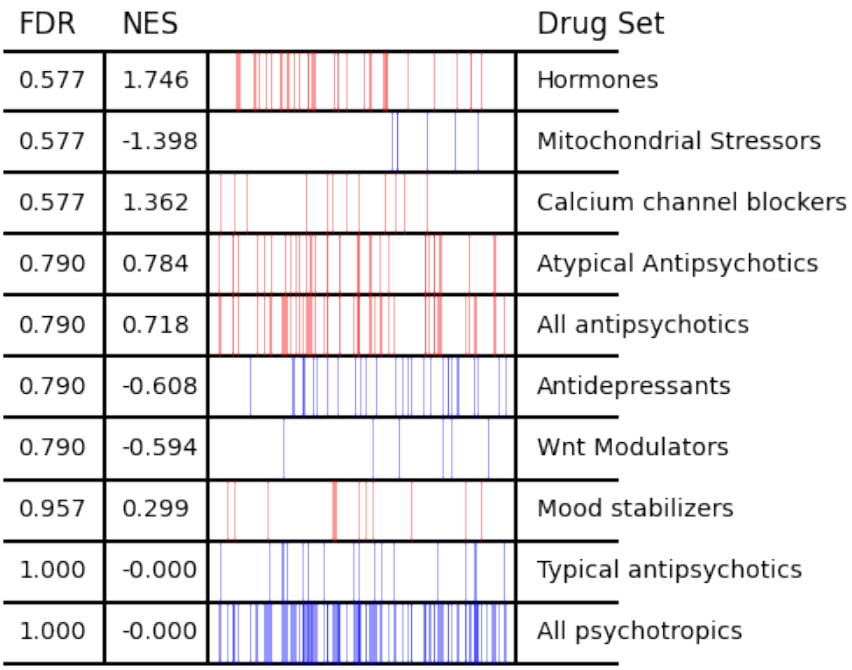

Supplementary Figure 5. Existing classes of psychoactive drugs do not, overall, show evidence of impacting mitochondrial localization (all doses). Data is shown as in main Figure 5, but here with each compound-concentration shown as a separate data point and with all classes shown. As an example, although the data in the first row appears skewed to the right, it does not show statistically significant rank ordering in the assay because the Mitochondrial Stressors class contains only a single compound.

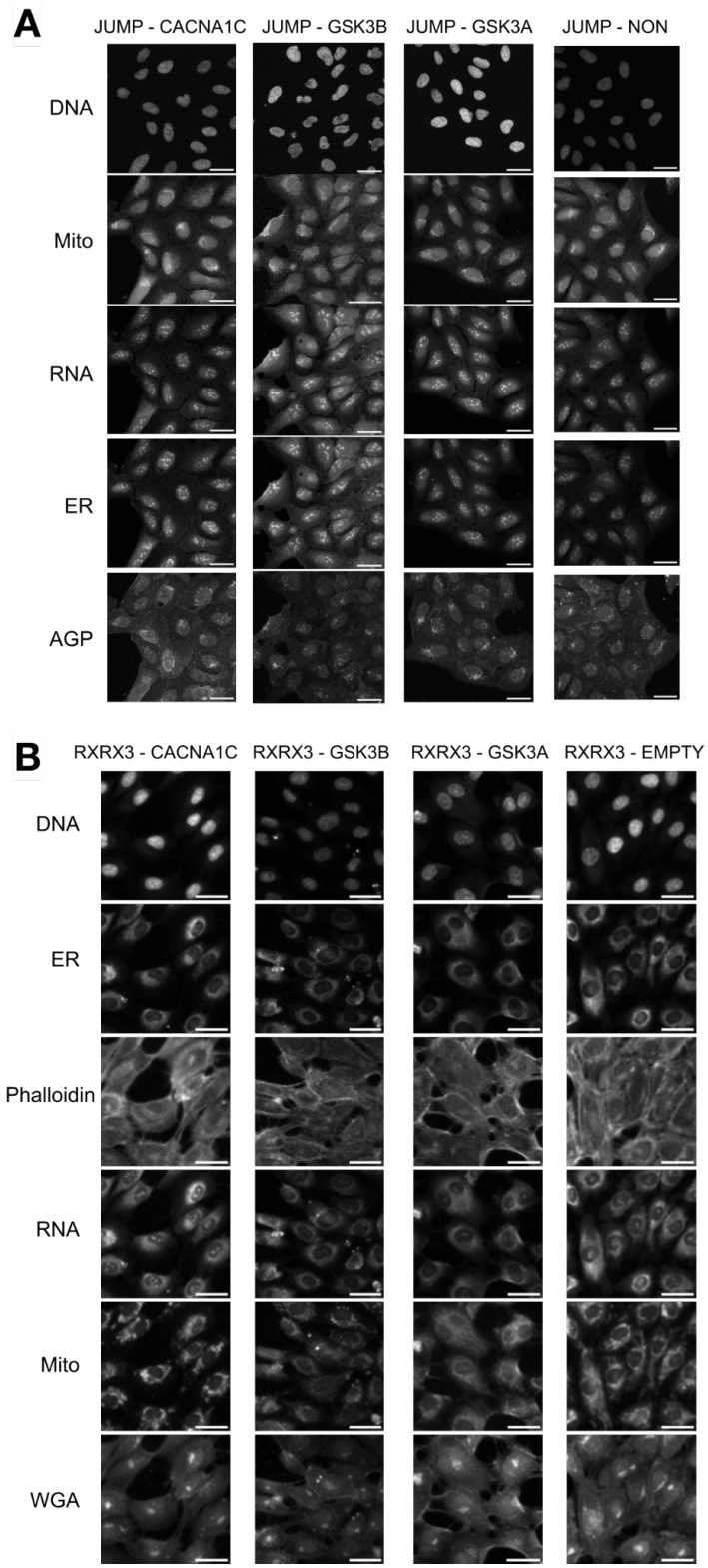

Supplementary Figure 6. Mitochondrial localization impact for genes with known association with mitochondrial function or psychosis - all channels. An additional field of view is shown for Figure 7, with all channels shown as grayscale. AGP = actin, golgi, plasma membrane (as in Cell Painting); WGA = wheat germ agglutinin. Scale bar = 50 μm.

Term	Adjusted P-va	Genes
Prolactin signaling pathway	0.048719663	MAPK9;SHC1;PIK3CB
Chronic myeloid leukemia	0.048719663	MECOM;SHC1;PIK3CB
ErbB signaling pathway	0.048719663	MAPK9;SHC1;PIK3CB
Growth hormone synthesis, secretion and action	0.048719663	MAPK9;SHC1;PIK3CB
Ras signaling pathway	0.048719663	MAPK9;SHC1;PIK3CB;ETS2

Term	Adjusted P-va	Genes
Insulin Signaling WP481	0.041629053	MAPK9;PFKL;SHC1;PIK3CB
Ras Signaling WP4223	0.041629053	MAPK9;SHC1;PIK3CB;ETS2
Prolactin Signaling WP2037	0.041629053	MAPK9;SHC1;PIK3CB
Osteoblast Differentiation And Related Diseases WP4787	0.04593157	MAPK9;IHH;PIK3CB
ErbB Signaling WP673	0.04593157	MAPK9;SHC1;PIK3CB
DNA Damage Response Only ATM Dependent WP710	0.04593157	MAPK9;SHC1;PIK3CB
Familial Partial Lipodystrophy WP5102	0.04593157	MAPK9;CIDEA

Supplementary Figure 7. Enrichment analysis of the 39 overexpression hit genes using Enrichr shows gene classes enriched for cell growth and cancer. classes . p-values are adjusted for multiple hypothesis testing and are borderline statistically significant; the analysis used the 15,000 tested genes as background. Analysis included many pathway libraries / ontologies; only KEGG (top) and WikiPathways (bottom) are shown; the remainder had no significant enrichments (Reactome, MSigDB, Hallmark sets, GO BP, GO CC, GO MF). Enrichment results files are available in the paper's Github repository here:
https://github.com/carpenter-singh-lab/2025_Haghighi_Mito/tree/main/results

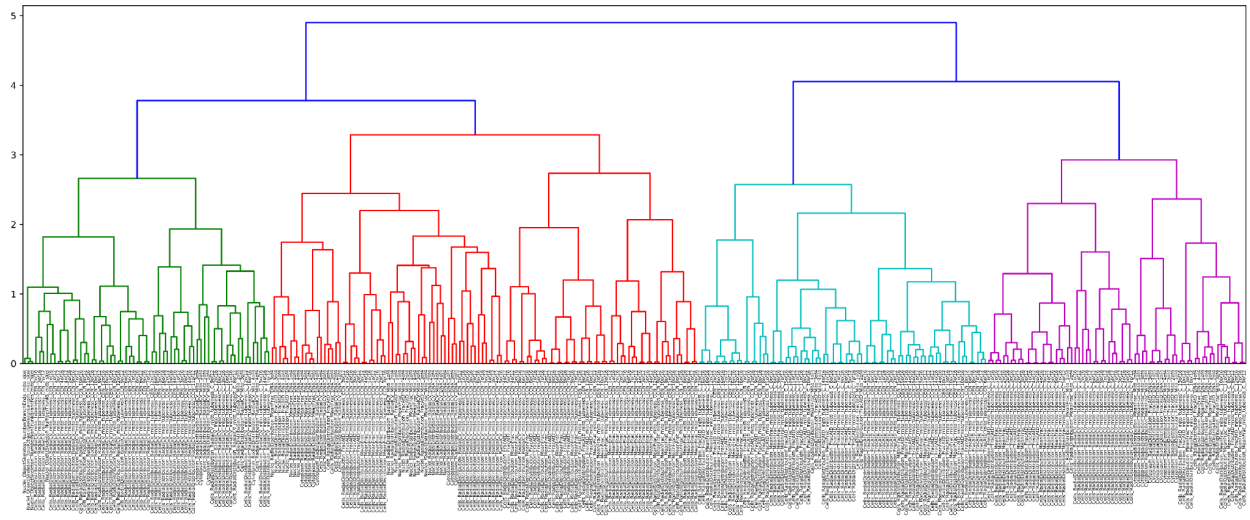

Supplementary Figure 8. Hierarchical clustering dendrogram of mitochondrial channel features used for feature selection. The dendrogram illustrates clustering of 326 CellProfiler-extracted mitochondrial features based on Pearson correlation. A height threshold was selected to form the maximum number of feature clusters while ensuring that the resulting representative features had a Variance Inflation Factor (VIF) < 10, mitigating multicollinearity. One feature per cluster (the median feature) was selected to form a reduced, interpretable feature set of 45 representatives used for feature importance analysis in classification tasks. A high-resolution version of this figure is available here: https://github.com/carpenter-singh-lab/2025_Haghighi_Mito/blob/main/results/dendrogram_mito.pdf

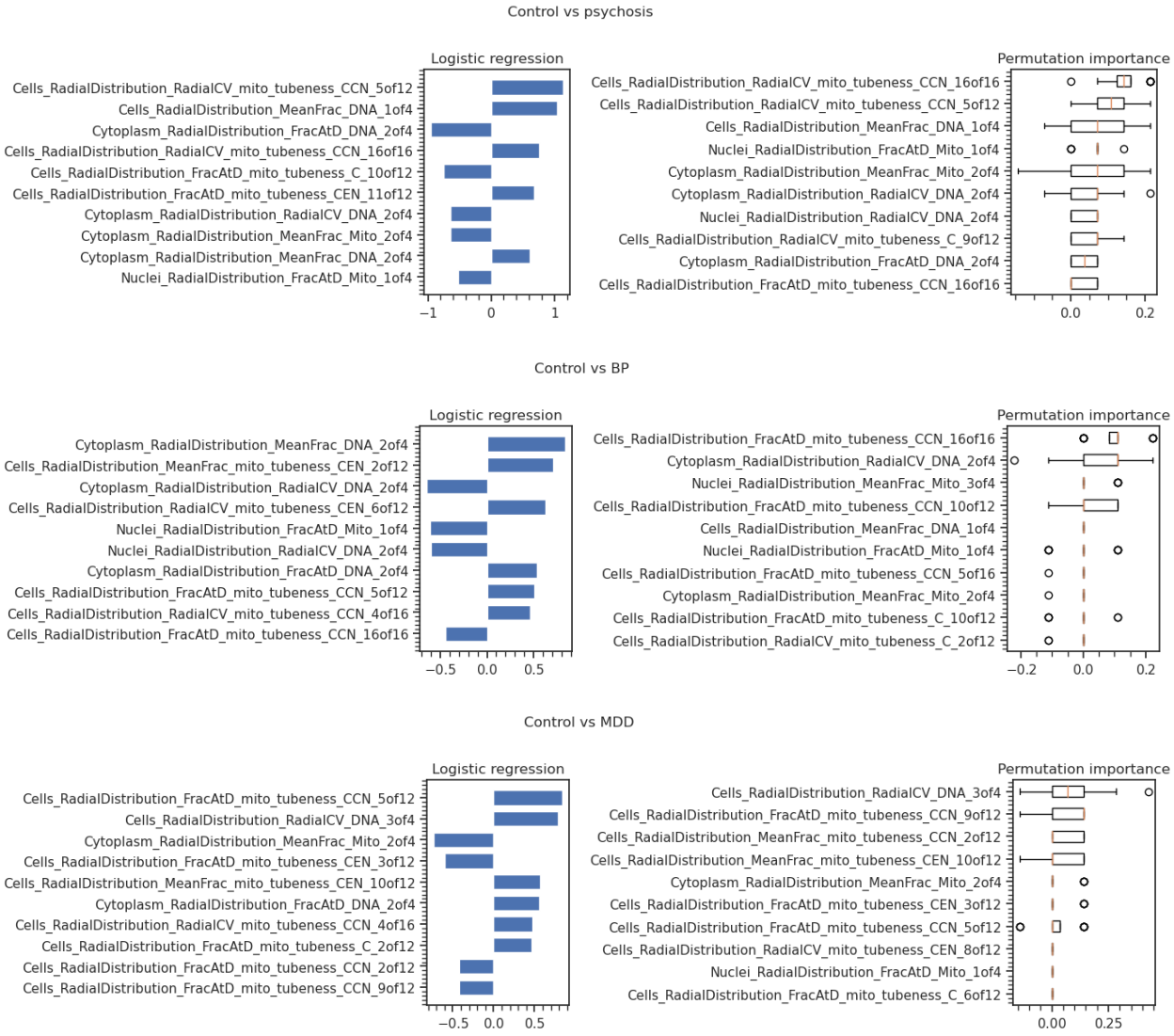

Supplementary Figure 9. Feature importance analysis for distinguishing patient subgroups from controls using logistic regression models trained on representative CellProfiler mitochondrial features. For each binary classification task (Control vs. Psychosis, BP, SZ, SZA, or MDD), models were trained using a reduced set of 45 decorrelated features selected via hierarchical clustering to mitigate multicollinearity. Shown are the top 10 features ranked by absolute model coefficients (left) and permutation importance (right), for subgroups with AUC-ROC > 0.6. Results highlight texture and intensity-based mitochondrial features particularly those capturing radial intensity patterns as key contributors to classification performance.